

Dynamic dispatch of solid oxide electrolysis system for high renewable energy penetration in a microgrid

Paolo Colombo^a, Alireza Saeedmanesh^b, Massimo Santarelli^a, Jack Brouwer^{b,*}

^a Department of Energy (DENERG), Politecnico di Torino, Corso Duca degli Abruzzi, 24, Torino 10129, Italy

^b National Fuel Cell Research Center, University of California, Irvine 92697-3550, United States



ARTICLE INFO

Keywords:

Renewable energy sources
Microgrid
Solid oxide electrolysis system
Dynamic dispatch
Hydrogen energy storage

ABSTRACT

The impacts of increasing deployment of Renewable Energy Sources (RES) on existing energy infrastructure has been investigated in a microgrid, an energy system that, with its constraints, foreshadows the challenges of the evolving electricity network. The campus microgrid of the University of California, Irvine (UCI) is modeled, including an existing natural gas-fueled combined cycle power plant, electric chilling and thermal energy storage, and analyzing the microgrid response to additional Photovoltaic (PV) installations. Open area on the campus of UCI can accommodate a maximum of 15 MW of fixed PV installation, and up to 22 MW of ground-mounted 2-axis tracking PV systems, providing together 37 MW of peak renewable capacity. The microgrid response to renewable installed capacity has been evaluated for different renewable installed capacity scenarios, ranging from the current 4 MW of installed capacity up to 35 MW. The results of the UCI microgrid analysis show that the RES penetration in supplying of the campus electrical demand could increase to 19% with the installation of 35 MW of PV, but 58% of the renewable production would be temporally in excess of demand and would have to be stored or curtailed, showing that a large-scale electrical energy storage system is required. A minimum aggregated power capacity of 300 kW of Solid Oxide Electrolysis (SOE) systems (the power capacity increment) is considered in the microgrid. The aggregate capacity is sized to absorb at least 80% of the excess annual renewable power production for each renewable capacity scenario, implementing a dispatch strategy able to respond to excess solar power available in the microgrid. The dynamic dispatch results of the modular SOE systems show that for cases with a renewable installed capacity higher than 15 MW, there is large excess electricity and so a great potential for hydrogen production. Almost 550 tons per year of hydrogen were produced for 35 MW of renewable installed capacity. The feasibility of on-site hydrogen utilization such as in the local hydrogen fueling station for fuel cell electric vehicles and the direct injection of the produced hydrogen into the gas turbine fuel inlet to reduce the natural gas consumption have been analyzed.

1. Introduction

The increasing distribution of RES [1–6] as a solution to environmental problems such as greenhouse gas and air pollutant emissions [7] has highlighted challenges related to their integration with the existing electric utilities' grid networks. Solar and wind energy are the fastest growing renewable energy sources [8,9], thanks to the significant reduction in their levelized cost of electricity [10,11]. However, the increasing trend in integration of RES presents issues related to their variable, intermittent and sometimes unpredictable nature, as well as temporal mismatch between energy demand and supply [12]. In the current situation, the variability of power demand and supply on the

grid can still be handled by the traditional grid structure in most of the cases ramping up or down fossil fueled power plants or turning on natural gas-fired peaking plants. In the near future, this could not be possible anymore because of high renewable penetration and technical limitations of traditional power generation.

With rapid rising of RES market penetration, continuous balancing of the grid is necessary to maintain stability, and to provide more flexibility and reliability to the system. Large-scale short- and long-term energy storage systems have an essential role in managing the power supply and demand which produces a more resilient energy infrastructure. Electrochemical energy storage systems (primarily lithium ion batteries) have grown in interest in the last decade as effective at

Abbreviations: APEP, advanced power and energy program; BoP, balance of plant; P2G, power-to-gas; PEM, proton exchange membrane; PV, photovoltaic; RES, renewable energy sources; SCE, Southern California Edison; SOE, solid oxide electrolysis; UCI, University of California, Irvine

* Corresponding author.

E-mail address: jbrouwer@uci.edu (J. Brouwer).

<https://doi.org/10.1016/j.enconman.2019.112322>

Received 26 May 2019; Received in revised form 14 November 2019; Accepted 18 November 2019

Available online 28 November 2019

0196-8904/© 2019 Elsevier Ltd. All rights reserved.

Nomenclature	
<i>List of Symbols</i>	
<i>E</i>	Energy (Wh)
η	Efficiency (%)
<i>HHV</i>	Higher Heating Value (kJ/kg)
<i>LHV</i>	Lower heating value (kJ/kg)
<i>LOAD</i>	Electrical or thermal demand (kW)
<i>m</i>	Mass (kg)
<i>P</i>	Power (W)
<i>T</i>	Temperature (K)
<i>X</i>	Volumetric fraction (Nm ³ /Nm ³)
<i>Subscripts</i>	
<i>El</i>	Electrical

both distributed and centralized scales, due to the absence of geographical constraints and good scalability due to a modular nature. Regarding long-term and large-scale energy storage at the electric utility grid network scale the electrochemical conversion of electricity into hydrogen via water electrolysis, called Power-to-Gas (P2G) concept [13–16], is a promising future solution. P2G technology consists of the electrochemical conversion of electricity and water into hydrogen. P2G is a flexible clean energy carrier that could provide massive electricity storage and facilitate the interconnection of the electric sector with other energy sectors, such as built environment demands, industry demands for high quality heat and chemicals (e.g., cement, steel, and fertilizer), and difficult-to-electrify transportation demands (e.g., aviation, long-haul trucking, shipping) [17–19].

P2G technology could provide interconnection and interdependence of gas and electrical networks as an effective solution to overcome high RES use energy sector challenges [20,21]. P2G can contribute as an energy storage solution to store massive amounts of renewable electricity and as a promising approach to decarbonization of the difficult-to-electrify parts of the economy by converting renewable electricity into a zero emissions fuel and feedstock [22]. P2G technology integrated with methanation could enable production of synthetic renewable methane to be injected in to the gas grid for large-scale and long-term storage [23–25].

The electrolysis process can be performed with three main technologies: proton exchange membrane electrolyzers, alkaline electrolyzers and solid oxide electrolyzers [26]. Today only the first two technologies present commercial grade solutions and a large number of installations are already in operation, while solid oxide electrolyzers are currently being developed and commercialized [27,28]. The high operating temperature of SOE systems, that is, 800–1300 K, eliminates the need for expensive catalysts and increases conversion efficiency and system integration opportunities. The high operating temperature also provides the possibility of utilizing available steam from other plants or utilizing available heat sources for water to steam conversion to reduce the required energy input to the SOE system.

The potential of P2G decentralized energy storage capability has been highlighted from the economical point of view compared to lithium-ion batteries for storage durations from 12 to 35 h. The efficiency-adjusted capital cost of P2G does not depend upon the storage size but only on the power output, since this kind of system can be integrated into the existing natural gas grid [29]. Hydrogen storage advantages compared to grid-scale batteries also derive from the lower manufacturing energy input per unit of stored energy that results, even with lower round-trip efficiencies, and in a better performance if the entire life cycle is taken into consideration [30]. Large-scale hydrogen energy storage is possible due to separate power and energy scaling

<i>EXCESS</i>	In excess with respect to the demand
<i>EXTRA</i>	Additional thermal energy
<i>GT</i>	Gas Turbine
<i>H₂</i>	Hydrogen
<i>IMPORT</i>	Electricity from external grid
<i>mix</i>	Mixture
<i>NG</i>	Natural Gas
<i>Out</i>	Outlet stream of the gas turbine
<i>ST</i>	Steam Turbine
<i>SCALED</i>	Increased proportionally to rated capacity
<i>Th</i>	Thermal
<i>Waste</i>	Thermal power of the gas turbine exhaust gas

engendering utility grid network scale storage of solar and wind power. Use of hydrogen energy storage has been shown to enable use of 100% wind energy use with hourly, daily and seasonal load shifting, and the advantage of the possible integration with local fuel cell electric vehicle fleets [31]. The renewable hydrogen can be converted back to electric power when needed in a fuel cell or in traditional reciprocating engines or gas turbines, or further converted to other chemicals, both gaseous or liquid, to be used as a liquid fuel or feedstock in the chemical industry [32–34].

The use of hydrogen storage systems in addition to the use of batteries in microgrids has grown in recent years. Plug and play in Chile is a microgrid that comprises a 125 kW solar PV facility combined with a hybrid energy storage system including 450 kWh of hydrogen storage and 132 kWh of lithium-ion storage [35]. Stone Edge Farm microgrid, located in Sonoma California, is another microgrid which uses the excess electricity to generate hydrogen from water and electricity to enable larger scale storage of energy at a lower capital cost than batteries [36]. It uses the generated hydrogen as a fuel cell vehicle fuel and as a source of electricity generation in the microgrid to generate 100% of its own peak demand and enable annual net zero electricity demand. The UCI microgrid is another microgrid which has a 60 kW P2G system based on a proton exchange membrane electrolyzer which produces renewable hydrogen from PV electricity that is injected into the natural gas system feeding a gas turbine combined cycle power plant [37]. For islands that are dependent upon primary energy importations with high costs, high RES penetration could be achieved with hydrogen storage [38]. The microgrid located on the small island of Utsira in Norway uses an integrated wind-hydrogen energy system which provides a continuous, and reliable energy supply, in which hydrogen is used as the energy storage medium [39].

The objective of this paper is to investigate and analyze the dynamic dispatch of the minimum required aggregated power capacity of 300 kW SOE unit systems into the UCI microgrid to store at least 80% of the excess solar renewable electricity that could be generated on the UCI campus in the form of hydrogen for different high RES penetration scenarios. The proposed SOE system, microgrid dispatch model, and SOE dispatch model are developed and simulated in Matlab. The paper simulates the dynamic behavior of the UCI microgrid plant considering all limitations associated with the various microgrid generation and load components (e.g., solar PV, gas turbine). It also simulates sequential dispatch of 300 kW SOE unit systems into the microgrid. In addition, the paper assesses the utilization of the produced renewable hydrogen blended with natural gas as a fuel in UCI microgrid combined cycle power plant as well as the use of hydrogen in a hydrogen fueling station.

2. System description

The system configuration has been developed to realize a stand-alone electrolysis system where the only energy input is electrical energy. Two inlet streams are present, the water stream and the ambient air stream. The system layout is shown in Fig. 1.

Water is fed to the system by a pump to provide sufficient head to overcome system pressure drops and is assumed to enter the system at 15 °C. Feed water is pre-heated to 100 °C by the two intercooling stages of the hydrogen compression section. Evaporation is then carried out recovering heat from both stack outlet flows and completed by an electric steam generator. The steam is further pre-heated in a counter-flow heat exchanger with the outlet hydrogen-rich flow and then mixed with the hydrogen-rich recirculated flow entrained by the recirculation ejector in order to obtain the required cathode inlet composition with 10% hydrogen molar concentration [40]. The final super-heating necessary to bring the steam to the required stack inlet temperature is performed by the steam side electric heater. After the passage through the stack channels, where the electrochemical conversion of steam into hydrogen takes place, a recirculation valve allows a split of the outlet hydrogen-rich mixture for partial recirculation. The main stream is then cooled down by the counter-flow heat exchanger and steam generator in order to recover its thermal energy. Additional cooling below 60 °C is performed in the water separator and the water is recirculated into the feed water flow. The pure hydrogen flow is then sent to the two-stage compression section with intercooling to reach a final outlet pressure of 30 bar adequate for natural gas pipeline injection.

On the sweep-gas side, ambient air is fed to the system by a blower, pre-heated by a counter-flow plate heat exchanger with the stack anode outlet and further heated to the required stack inlet temperature by an electric heater. Crossing the stack, the flow is enriched by oxygen coming from the cathode side and then is used to pre-heat the entering air and contribute to the steam generation before being discharged to the environment. Modeling details of both stack and Balance of Plant (BoP) components as well as the control scheme were explained in detail in [41].

It should be noted that in each SOE unit system, 2500 unitary

cathode-supported (fuel electrode-supported) planar square-geometry cells with an active surface area of 100 cm^2 are assumed to be assembled into several unit stacks to comprise a 300 kW (nominal power) SOE stack module. In this study, electric power consumption in the range of 120 kW–480 kW (20% to 160% of the 300 kW nominal stack power) is considered for the stack of each SOE system module. The maximum efficiency of this stand-alone SOE system was found to be 75% on an LHV basis, which is consistent with the literature [42]. Minimum operating power of a single SOE stack module is determined to have at least 50% system efficiency. Also, maximum operating power of a single SOE stack module is determined to correspond to a maximum cell voltage of 1.35 V to prevent voltage degradation.

Fig. 2 shows system efficiency and hydrogen production rate versus system electric power consumption for the developed system obtained from a step-wise dynamic simulation. As Fig. 2 shows, the SOE stack module operating power range has been limited to working conditions that allow production of hydrogen with an overall system efficiency above 50%, which is a typical system efficiency value of competing electrolysis technologies like PEM and Alkaline [43]. The electrolysis efficiency of the SOE system is higher due to thermodynamic advantages of performing high temperature electrolysis, which include lower open circuit voltage, and lower overpotentials due to better kinetics that allow higher operating current density directly proportional to hydrogen production at a given electric power input [44].

It should be noted that the drop in system efficiency below 250 kW and above 550 kW of system power (Fig. 2(a)) is due to the way that the SOE stack thermal controller works to keep the SOE stack operating temperature inside the required safety range, as discussed in [41]. For system powers below 250 kW the electrolysis stack is operated in strongly endothermic conditions and additional heat must be supplied to maintain cell temperatures inside the desired operating range. System working powers above 550 kW correspond to strongly exothermic operation of the electrolysis stack. In both situations the air blower begins pushing more air through the SOE stack to manage its temperature, which causes an increase in air blower and air electric heater power consumption. This increase of auxiliary power consumption results in the observed drop of overall system efficiency.

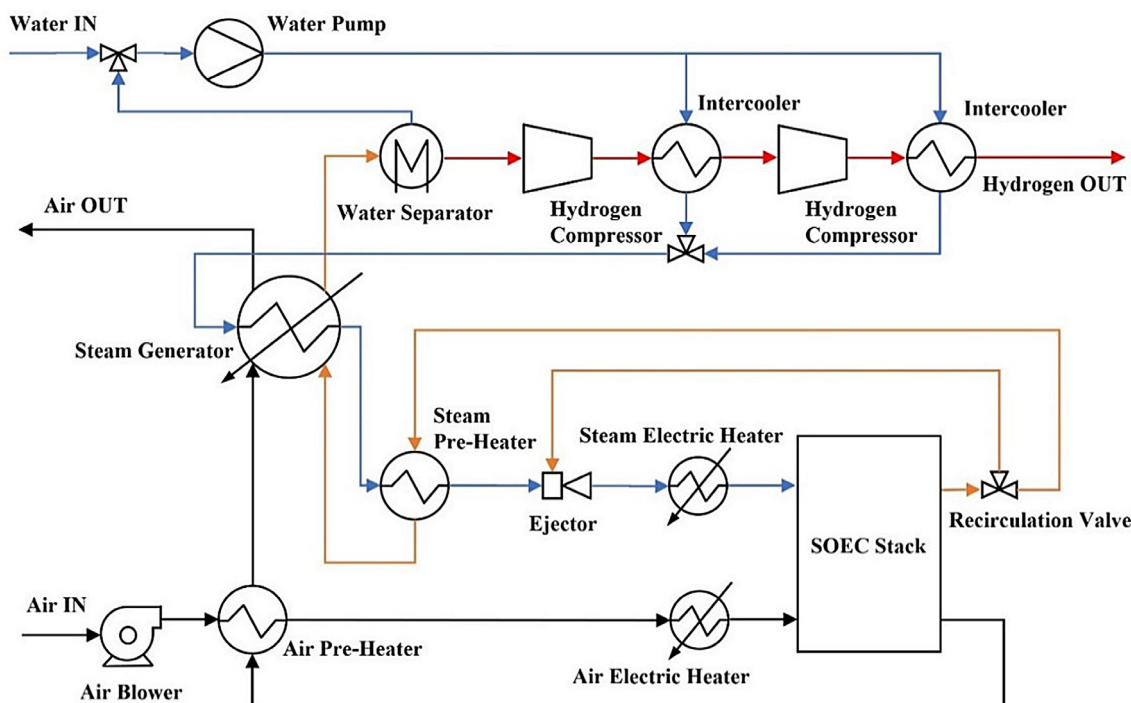


Fig. 1. SOE unit system layout.

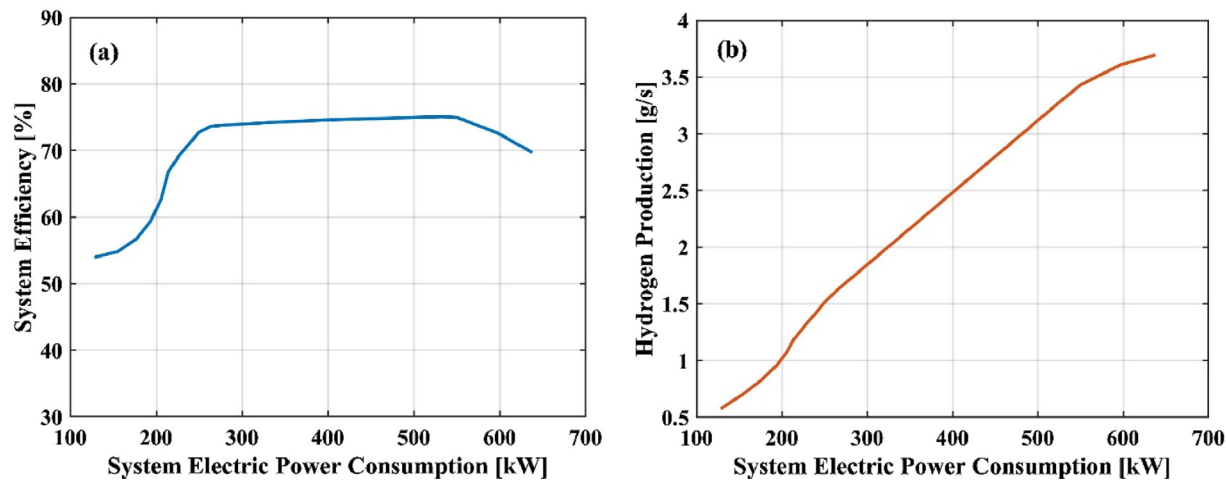


Fig. 2. (a) SOE unit system efficiency, and (b) hydrogen production rate versus SOE unit system electric power consumption.

3. UCI campus microgrid

The University of California, Irvine campus offers a unique opportunity to investigate the management and performance of a microgrid. The microgrid presents a variety of building types such as classrooms, laboratory facilities and offices and also some features that are going to become part of future energy systems such as electric vehicle and bus fleets and their charging stations, chemical batteries for grid balance, and a large set of renewable distributed energy generation resources (mostly solar PV) [45]. The campus microgrid is connected with the external Southern California Edison (SCE) grid through a single substation where the voltage is decreased from 66 to 12 kV. The campus power plant is able to provide more than 90% of campus electricity consumption via ten 12 kV circuits and district heating and cooling network. The power plant consists of a 19 MW natural gas-fired combined cycle formed by a 14 MW gas turbine and a 5 MW steam turbine, 7 electrically driven chillers and 1 steam driven chiller. One of the main characteristics of the UCI central plant is the presence of a 175 MWh cold water storage tank and cold water distribution to all major campus buildings that allows the microgrid management to produce campus air conditioning via the chillers during at any time of day or night (e.g., at off-peak hours or when solar is available in excess) [46].

On the UCI campus, following the plan of the University of California to achieve carbon neutrality in 2025, there are already in operation three large PV installations over parking structures and many other distributed rooftop installations for a total installed capacity of about 4 MW and two two-axis tracking concentrated solar-PV systems of 113 kW installed capacity. These solar installations, coupled with deep energy efficiency measures deployed throughout the campus, are already introducing challenges to the microgrid operation when the power plant output has to adjust to very low power levels to allow renewable energy utilization in the microgrid. Given the future goal of UCI administration to increase the renewable share of the energy mix, the implementation of energy storage will become a fundamental requirement of the campus energy infrastructure.

In this paper, the implementation of a P2G system based upon dispatching SOE unit systems is investigated. Fig. 3 shows the existing microgrid components in addition to current proposed use of the SOE unit systems (dashed lines).

4. Microgrid demand profiles

Historical data regarding the campus demand and PV production from the year 2014 have been provided by UCI facilities management and used as inputs in this study. The data come with a 15 min-resolution and include both electricity and thermal demand. The campus

electric and thermal loads are presented in Fig. 4.

The campus annual electric demand was around 126 GWh in 2014 with an average load of 14.32 MW, a maximum load of 27.7 MW and a minimum load of 9.2 MW. Electricity demand is quite uniform (primarily because of careful control of the chillers and thermal energy storage system) during the year presenting daily peaks in work days and decreasing over the weekends. The highest electrical consumption days usually coincide with the hottest days when the electrical demand for campus air conditioning is highest. Campus thermal demand varies between 5 and 27 MW and shows a significant seasonal variation rising during the winter and generally decreasing over the summer. The PV installed capacity in 2014 represented by the data was 893 kW and PV power demand dynamics have been scaled up for all of the future simulation scenarios using a scaling factor as illustrated in Eq. (1), in order to simulate the grid response to increasing renewable installed capacity.

$$PV_{ScaleFactor} = \frac{\text{Future installed capacity}}{\text{Installed capacity (2014)}} \quad (1)$$

Previous work at the Advanced Power and Energy Program (APEP) at UCI estimated that a maximum of 15 MW of fixed PV installations (mainly on building rooftops, parking structure terraces, and above parking lots) and up to 22 MW of ground mounted 2-axis tracking PV systems (37 MW in total) could be installed in and/or nearby the UCI campus [45].

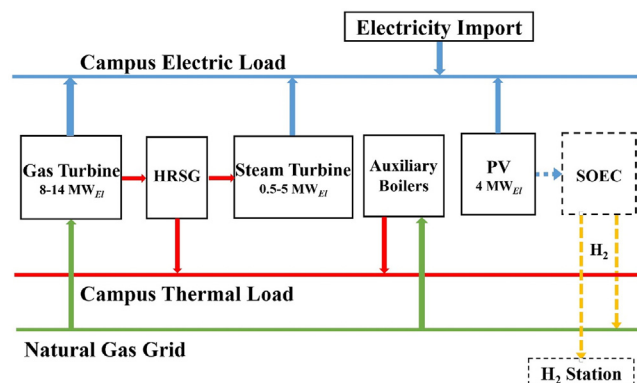


Fig. 3. Schematic representation of microgrid components considered in this analysis and SOE unit systems integration.

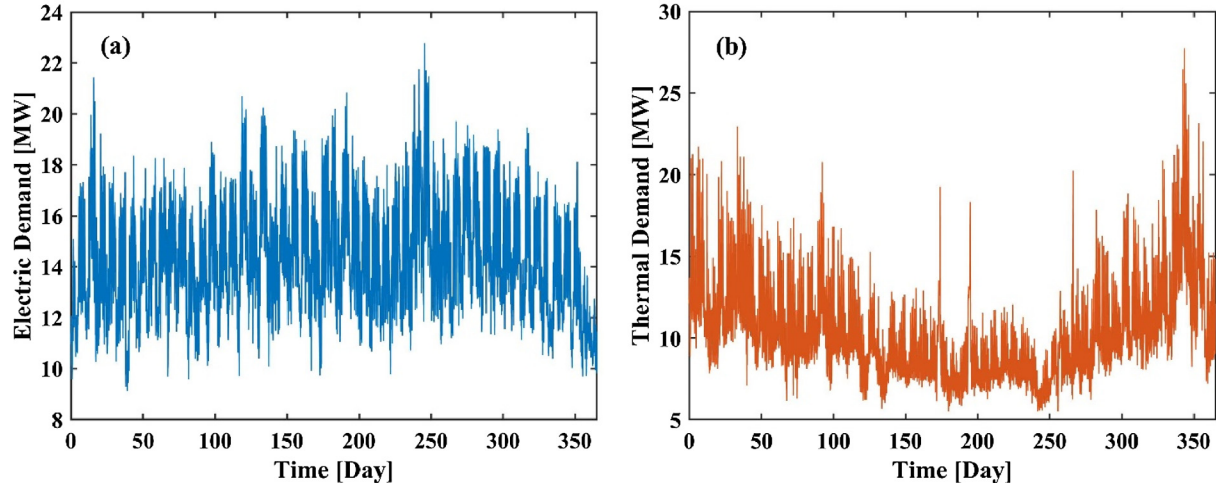


Fig. 4. UCI campus (a) electricity demand, and (b) thermal demand for the year 2014.

5. Microgrid power plant model

The Gas Turbine is the main component of the campus power plant. The maximum electrical power output is 14 MW and the turbine can be turned down to a minimum power output of 8 MW; the minimum operating point is a consequence of necessary compliance with the strict criteria pollutant emissions laws of the state of California. Moreover, in this study, the gas turbine is constrained not to ramp faster than 6 MW/h [46].

A simplified regression based gas turbine model has been previously developed [47], and has been implemented to simulate the operation of the campus power plant. The gas turbine electrical efficiency ($\eta_{GT,El}$) and turbine exit temperature ($T_{GT,Out}$) are correlated to the electrical power output ($P_{GT,El}$) according to Eqs. (2) and (3), represented in Fig. 5 for a range of the gas turbine electrical power outputs.

$$\eta_{GT,El} = f(P_{GT,El}) = -8.9 \times 10^{-4} \times P_{GT,El}^2 + 0.0299 \times P_{GT,El} + 0.0833 \quad (2)$$

$$\begin{aligned} T_{GT,Out} &= g(P_{GT,El}) \\ &= 0.069 \times P_{GT,El}^4 - 2.12 \times P_{GT,El}^3 + 19.14 \times P_{GT,El}^2 - 31.57 \\ &\quad \times P_{GT,El} + 636.27 \end{aligned} \quad (3)$$

According to Fig. 5, the electrical efficiency of the turbine decreases from 33% at the maximum operating load to 26% when the turbine operates at the minimum electric power output of 8 MW. On the other

hand, the temperature of the turbine outlet increases from 764 K (at maximum load) to 811 K when the turbine is turned down to the minimum load.

The thermal power available from the turbine exhaust for the heat recovery steam generator is evaluated using Eq. (4) which takes into account the ratio between the difference between $T_{GT,Out}$ and temperature of gases leaving the steam generator (450 K) and the difference between $T_{GT,Out}$ and the reference temperature (273 K) at which heating values are evaluated.

$$P_{GT,Th,Waste} = P_{GT,El} \times \frac{(1 - \eta_{GT,El})}{\eta_{GT,El}} \times \frac{T_{GT,Out} - 450}{T_{GT,Out} - 273} \quad (4)$$

This thermal energy in the form of steam is then used in the co-generation plant to feed the steam turbine and to cover the campus heat demand via steam/purified water heat exchangers.

The 5 MW Steam Turbine never operates at full load since it is oversized for the application. Also, the minimum operating power is 0.5 MW to avoid the risk of an electrical trip if the campus were to suddenly draw additional steam for heating. Moreover, it can be turned on and off depending upon electric demand and steam availability [48]. During emergencies the turbine can respond to transients as fast as 1 MW/min, though standard operation limits manipulation to a rate of approximately 4 MW/h [46]. In every moment the maximum possible electrical output that can be delivered by the recuperative steam turbine is then related to the available waste heat by the electrical efficiency $\eta_{ST,El}$ according to Eq. (5).

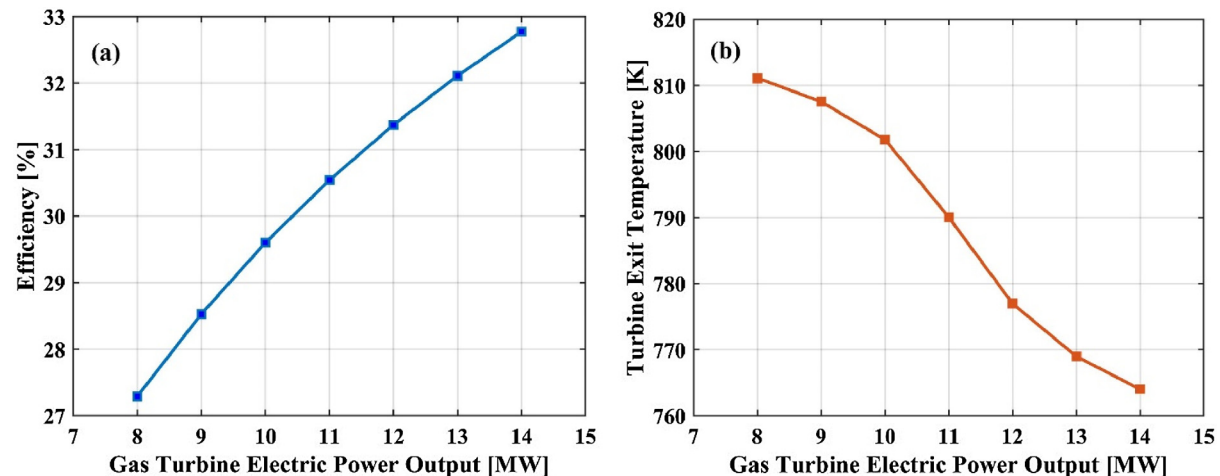


Fig. 5. Gas turbine regression based operating parameters: (a) efficiency, and (b) turbine exit temperature.

$$P_{ST,El} = P_{GT,Th,Waste} \times \eta_{ST,El} \quad (5)$$

Steam turbine will operate when excess steam is available to minimize the import power level to the campus, as long the minimum import restriction will not be violated. During periods in which the waste heat from the gas turbine is not sufficient to cover the campus heat demand, additional natural gas can be burned with the use of duct burners to raise the temperature of the exhaust gas [49]. The operational parameters and assumptions of the microgrid model are summarized in [Table 1](#). It should be noted that a minimum import of 100 kW (from external grid) is considered as a constraint in the model because, in real life, it is extremely inefficient and unavailable to turn on and off the import of power when desired [50].

6. Microgrid dispatch model

The dispatch of the microgrid energy resources has been simulated as a linear programming problem implemented in Matlab®. In the linear programming, variables are linked together with linear constraints and upper and lower boundaries must be set. The problem variables include the electrical power output of the gas turbine ($P_{GT,El}$), the amount of waste thermal power in the form of steam fed to the steam turbine ($P_{ST,Th}$), the extra natural gas power needed to satisfy thermal demand ($P_{EXTRA,Th}$), the electrical power import from external grid ($P_{IMPORT,El}$), the possible electric power excess ($P_{EXCESS,El}$) and the waste thermal power still available from the gas turbine outlet that is not being recovered ($P_{EXCESS,Th}$).

The electrical and thermal power balances, shown in Eqs. (6) and (7), are constraints that must be satisfied at every time step:

$$P_{GT,El} + P_{ST,El} + P_{IMPORT,El} - P_{EXCESS,El} = LOAD_{El} - P_{PV,El,SCALED} \quad (6)$$

$$P_{GT,Th,Waste} - P_{ST,Th} + P_{EXTRA,Th} - P_{EXCESS,Th} = 1.1 \times LOAD_{Th} \quad (7)$$

It should be noted that a coefficient of 1.1 is considered in the thermal load energy balance to take into account all the heat losses to the environment (distribution/piping heat losses) [51].

The objective function reflects the current dispatch strategy of the UCI microgrid, oriented to maximize the utilization of the solar PV and combined cycle plant thus minimizing imports of electrical power from Southern California Edison grid and using additional natural gas to cover thermal demands.

7. SOE unit systems dispatch

The integration of SOE unit systems into the campus microgrid has been simulated as the deployment of multiple identical SOE unit systems as described previously. The annual excess electricity profile of the UCI microgrid obtained from the microgrid dispatch model is the SOE input parameter. The otherwise curtailed electricity available at every time step is supposed to be delivered to the SOE unit systems which supplies both the SOE stack and BoP components. In this study, the SOE units are designed to stay in a hot idle state when not in operation: energy consumption during the idle periods has not been taken into account, but it has been estimated for a similar system that a 30 cm insulation layer is enough to keep overnight temperature decrease negligible without additional active heating [52]. A sequential dispatch strategy has been developed and described in this study. When excess electricity from PV production is available on the microgrid, the SOE units are turned on sequentially one after the other. The units are turned on when the amount of excess electrical power is higher than the power consumption of the single SOE unit system at its minimum operating power of 120 kW. When the maximum load of the single SOE unit system is reached, the optimization allows some curtailment until enough power is available to turn on the next unit. With this dispatch strategy every unit works at full load except the last one that has been turned on, which works at part load. In the case of decreases of excess electrical power, the switch off procedure follows the opposite

symmetrical sequence.

8. Results

8.1. Microgrid operation

The microgrid dispatch results are summarized in [Fig. 6](#), highlighting the contribution of the available electrical energy sources to the annual electricity demand of the campus, from the current situation of 4 MW of PV installed capacity to the maximum local estimated capacity of 35 MW. The dashed line represents the percentage of the energy produced by the future PV installations that cannot be absorbed by the microgrid and that which would have to be curtailed or stored in the form of hydrogen using P2G technology. According to [Fig. 6](#), currently the campus combined cycle plant provides around 94% of the campus electrical needs, 83% of electricity production comes from the gas turbine and 11% from the steam turbine. The PV production can be fully absorbed by the microgrid and covers 5% of the annual campus electricity demand in a low PV installed capacity scenario. The imported electricity from the external grid is needed to supply only 1% of the electrical demand.

The general trend is obviously the increase of RES penetration as the installed PV capacity increases with consequent decrease of gas turbine and steam turbine contributions. The electricity import from the external grid shows a slight decrease but stays around 1% because of the current interconnection agreement that imposes a continuous minimum import.

The intrinsic limits of the microgrid structure, due to the power plant operation constraints, start to show as the amount of solar energy that would have to be curtailed or stored immediately starts to increase as the PV installed capacity increases (shown as excess percent of PV power). Installing new capacity up to 15 MW would result in sensible increasing in RES contribution from 5 to 15%, keeping solar excess around 20% of the production. Scenarios with further increasing of PV capacity show that only a 4% increase of RES is achieved up to 19% if the installed capacity increase from 15 MW to 35 MW. In the same range the percentage of excessive PV production that would have to be curtailed or stored increases from 20% to 58%.

[Fig. 7](#) shows the distribution of excess of PV power in terms of entity and frequency. On the y-axis there is an indication of the number of hours of the year during which the excess power is at least the value that can be read on the x-axis. The six lines correspond to scenarios with increasing PV capacity. The intercept points with the y-axis are the total number of hours with curtailment while the intercept points with the x-axis represent the annual maximum value of excess power. It can be highlighted that the peak power evolves linearly with the increase of installed capacity while the number of excess hours increase rapidly for scenarios up to 15 MW and then the growth slows down converging to the total number of hours of PV production meaning that the additional capacity cannot be handled by the grid in most of the hours with solar irradiation. The massive excess power can be noticed as the general trend of how the curvature of the curves changes moving toward higher PV capacity scenarios and much more hours have excess power closer

Table 1
Summary of microgrid model parameters [46,48].

Microgrid model parameters			
Gas Turbine	Electric output range	8–14	MW
	Electrical efficiency, $\eta_{GT,El}$	$f(P_{GT,El})$	–
	Turbine exit temperature, $T_{GT,Out}$	$g(P_{GT,El})$	K
	Ramp rate	6	MW/h
Steam Turbine	Electric output range	0.5–5, off	MW
	Electrical efficiency, $\eta_{ST,El}$	0.25	–
	ramp rate	4	MW/h

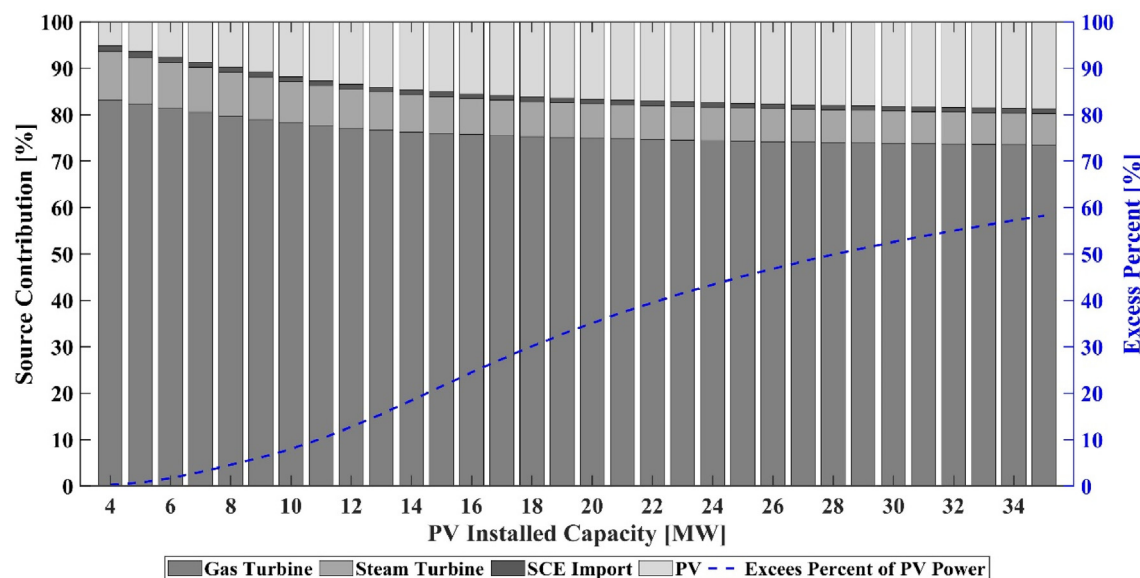


Fig. 6. Annual UCI microgrid electric energy generation mix and excess electricity in future scenarios with increased PV installed capacity.

to the maximum than to the minimum value.

8.2. Microgrid operation integrated with SOE unit systems

Simulations of microgrid operation integrated with SOE unit systems have been performed for the current situation and for future scenarios with increasing PV capacity installed, to investigate the microgrid and P2G system behaviors to accommodate additional solar energy production and its limits. In this study, annual simulations have been performed to calculate the annual percentage of otherwise curtailed excess electricity which is stored in the form of hydrogen. Fig. 8 shows the percentage of stored excess electricity versus the total power capacity of dispatched 300 kW SOE systems for different PV capacity scenarios. The percentage of stored excess electrical energy increases with an increase in the aggregated power capacity of dispatched SOE systems. For each PV capacity scenario, the aggregated power capacity of 300 kW SOE unit systems deployed varies between 300 kW (one SOE system) to a maximum aggregated power capacity required to store

nearly 100% of the excess electric energy during the analyzed year. According to Fig. 8, the percentage of stored excess electricity increases nearly linearly with the combined power capacity of dispatched 300 kW SOE systems up to 80% of total electric energy stored. For 35 MW of solar PV capacity, 6 MW of SOE systems are required to store about 80% of annual excess electricity while more than twice that power (12.3 MW of SOE systems) is required to store all the excess electrical energy. This non-linear behavior results from the fact that to store nearly 100% of the annual surplus of renewable electricity, the storage system needs to cover the very highest peaks of otherwise curtailed renewable electricity, which occurs infrequently. That is, these later added SOE systems have low capacity factor. In this study, the minimum aggregated SOE systems power capacity (minimum number of dispatched 300 kW SOE systems) that is simulated for each PV capacity scenario is the minimum total power required to store at least 80% of otherwise curtailed excess electricity. Only scenarios with installed PV capacity higher than 10 MW are reported here because lower capacities resulted in electricity excess that does not occur on a daily

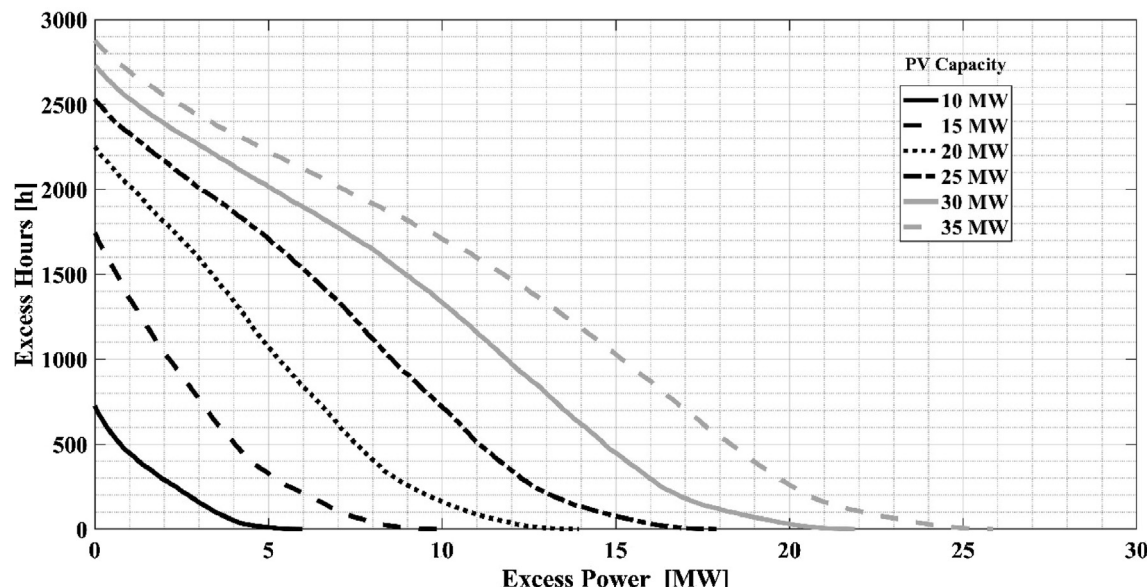


Fig. 7. Excess power distribution in future scenarios with increased PV installed capacity.

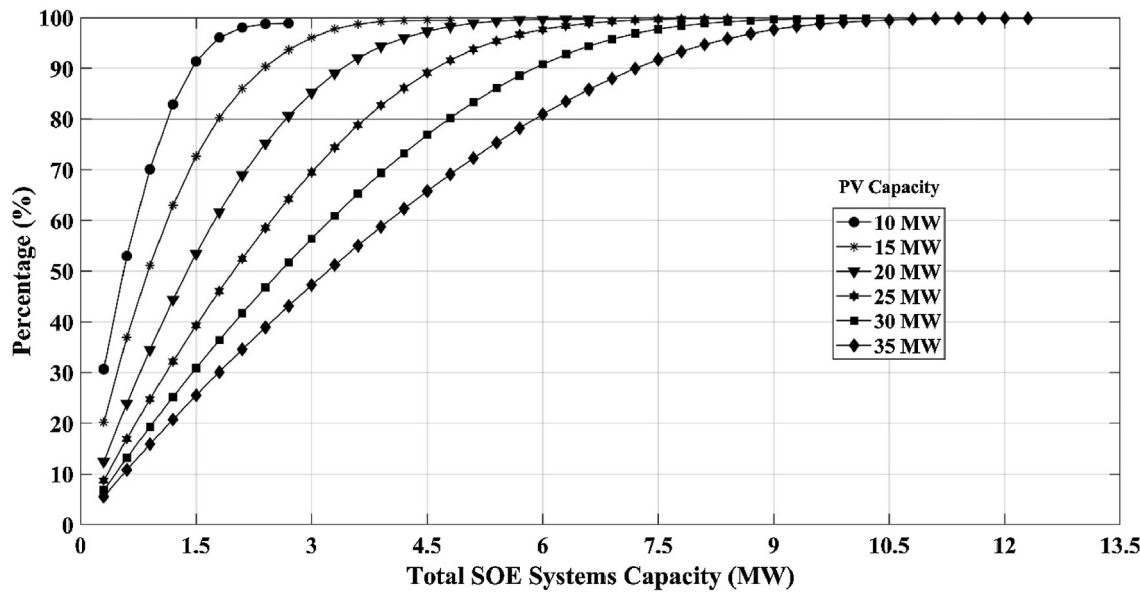


Fig. 8. Percentage of stored excess electric power via P2G vs. total power capacity of dispatched 300 kW SOE unit systems for different PV installed capacity.

basis.

Two representative weeks of operation for the current installed PV capacity of 4 MW are explained and shown in Figs. 9 and 10. Fig. 9 shows a week in September characterized by high electric demand and relatively low thermal demand. It can be clearly noticed that the weekly electric demand behavior with daily peaks during work days and a general decrease over the weekend when most of campus work activities are suspended. This week shows the ideal operation of the combined cycle plant, the gas turbine works at maximum load (and highest thermal efficiency) most of the time and, since the campus heat demand is low, the steam turbine is also able to be employed to cover electric load. The fluctuation of the steam turbine output, even when full electricity production would be requested, is complementary to the fluctuation of heat demand since priority on heat recovery is given to the campus thermal load. The daily PV production can be clearly identified with its peak in the middle of every day close to the maximum nameplate capacity of the current situation. September 5 shows an irregular shape of the PV production probably due to temporary cloud cover. During this chosen week the electrical demand is particularly high overcoming the electricity production of both the campus power plant and PV installations and, as a consequence, electricity import from the external grid is present during the first four days and reaches values around 2 MW. Substantial turn down of the combined cycle plant can be noticed during September 6 and 7 as a consequence of low electricity demand and high PV production forcing the power plant to reach close to the minimum operating condition of the gas turbine (8 MW) during September 7; in this case the fast ramps are provided mainly by the steam turbine, given the availability of recovered heat. It can be clearly noticed that during this week the PV production is beneficial because it mainly reduced the otherwise high electricity demand from grid imports. Also, in the represented week, there is no excess PV power to be stored or curtailed and as a result the amount of both P2G power and curtailment are zero. According to the Fig. 9(b), most of the time in the represented week, the steam turbine consumes most of the available heat recovered from the gas turbine exhaust gas in the heat recovery steam generator. In September 7, when the gas turbine reaches its minimum operating condition in the middle of the day, we have excess thermal power since the steam turbine steam consumption begins decreasing as a result of an increase in solar PV power. Also, according to Fig. 9(b), there is no need for the extra thermal heat in the represented September week since thermal demand is relatively low and can be supplied completely with heat recovered

from gas turbine exhaust gases in the heat recovery steam generator.

A week in January is presented in Fig. 10 showing a relatively lower electrical demand while the campus thermal demand is much higher and presents large peaks at the beginning of every day. During the first four days these peaks reach 20 MW making it impossible to be satisfied completely by heat recovery from the gas turbine even if it works at maximum load and the steam turbine is turned off. Additional natural gas must be burned in the auxiliary boilers present in the power plant every morning, as can be noticed in the lower portion of the Fig. 10(b). Moreover, since the steam turbine is not covering its part of electrical load because of the unavailability of steam for power generation, electricity import is also present during those mornings. Nevertheless, even during this week the PV production is well matched with the campus electrical demand, reducing considerably the electricity that would need to be imported since the heat recovery into the steam turbine is not possible as a consequence of relatively high heat demand. Similarly to the represented week in September, in the represented January week, PV power is not in excess and does not need to be stored via P2G or curtailed. Due to the priority given to the thermal demand of the campus, high for most of the time in January, the steam turbine consumes a small portion of the heat recovered in the form of steam in the heat recovery steam generator. In Fig. 10(a), at the end of January 8, we can see a moment in which the steam turbine is turned off because of decreasing electrical demand and as a result it does not consume any steam provided by heat recovered from the gas turbine. Consequently, since the thermal load is not high at that moment, we see an excess of thermal energy available.

According to Fig. 10(b), this represented week needs more heat compared to the available excess heat. Also, in comparison to the analyzed September week which has lower thermal demand, the steam turbine works at lower power output since the priority of the microgrid is to provide the thermal demand of the campus with the recovered gas turbine heat which is higher in January.

The second scenario presented is the case in which 10 MW of peak PV capacity is installed on the UCI campus, which is more than double the amount currently installed. The same two weeks of demand and solar availability used in previous analyses (Figs. 9 and 10) are reported in Figs. 11 and 12 to analyze the differences in microgrid response with the added PV. In Fig. 11, it can be noticed that now the peak power output from the PV is around 8 MW. More flexibility is requested of the gas turbine since every day the turbine has to ramp down as the PV output rises in the morning and ramp up as it decreases later in the

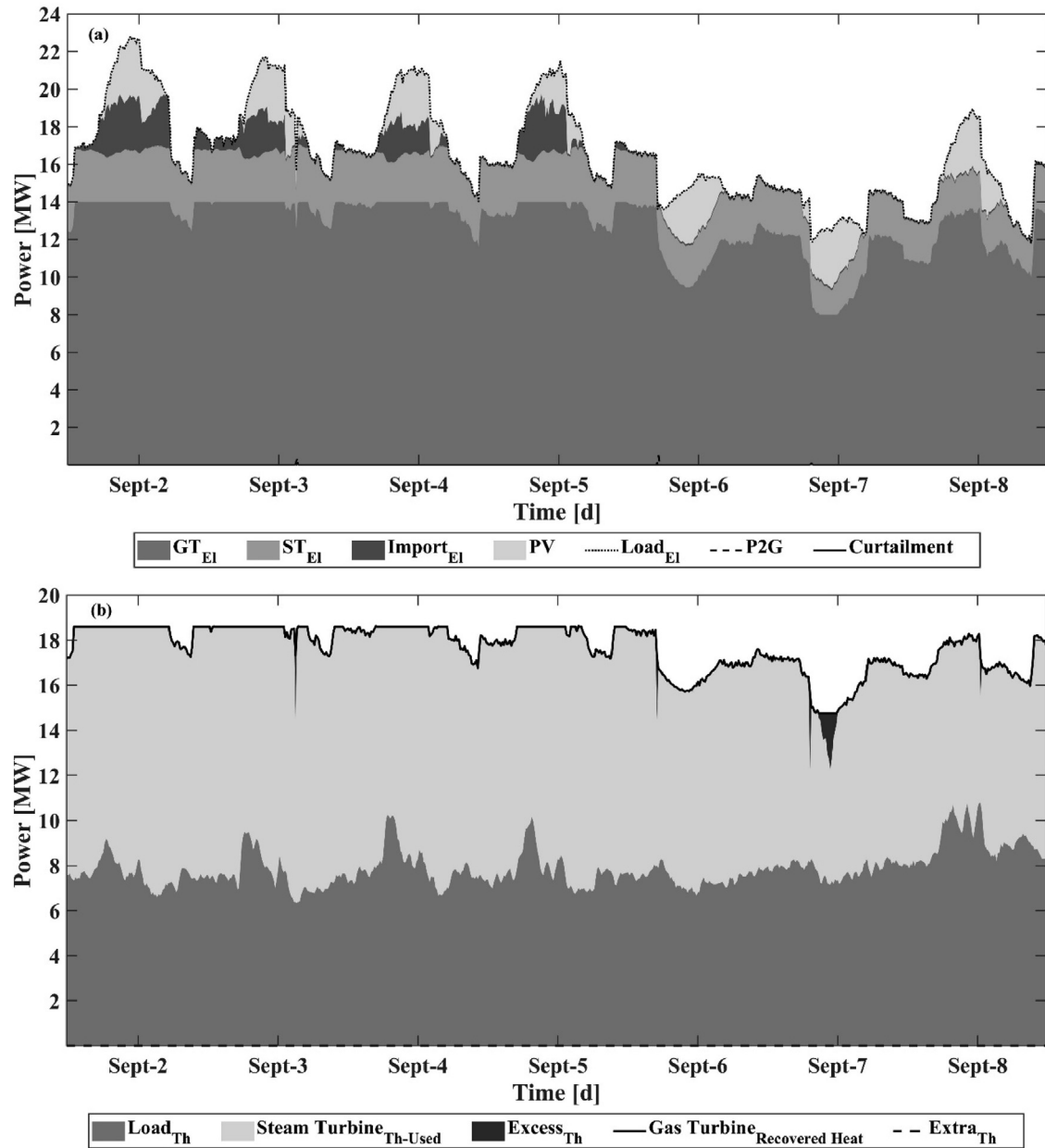


Fig. 9. Microgrid-SOE dispatch simulation results in a week of September (a) electric power balance, and (b) thermal power balance with the current 4 MW of PV installed capacity.

afternoon. During the days with high electricity demand these fluctuations are still inside the microgrid limits and the additional PV capacity leads to reduced electricity import and reduced natural gas consumption in the gas turbine plant compared to the 4 MW of peak PV case. As the electrical demand drops during the weekend, the first episodes of important excess power occur on September 7 in which the steam turbine is turned off and the gas turbine works at the minimum power output of 8 MW but up to 4 MW of excess PV electric power is produced during the day since the power production exceeds the microgrid demand. Since the aggregated power capacity of dispatched 300 kW SOE units was determined to store around 80% of the excess PV power, it can be seen that in the middle of the day on September 7, the P2G consumed power reaches its maximum design capacity and as a result a portion of excess power cannot be delivered to the SOE units and stored as a hydrogen fuel and has to be curtailed. Also, on that same day, we have up to 8 MW of excess heat during the day since the steam turbine is turned off and the recovered heat is much larger than the

campus thermal load.

Regarding the week in January shown in Fig. 12, the same response of the power plant to incoming PV production can be noticed throughout the week and again during work days the electrical demand is high enough to avoid complete gas turbine turn down while during the weekend excess PV power would occur. It can be also noticed that during days with cloudy weather, as in January 5 and 9, strong dynamics have to be imposed to the campus power plant to compensate for the loss of PV production. The resulting ramp rates are still achievable by the gas turbine alone in this scenario, since the high thermal demand prevents the utilization of the steam to drive the steam turbine. Moreover, in both the weeks reported it can be highlighted that, as the power output of the campus power plant decreases to accept PV production, the fact that the steam turbine is turned off leaves large amounts of heat available to recovery from the gas turbine exhaust when the campus thermal demand is not particularly high: in particular during the days of January 10 and 11 the excess of electricity and heat

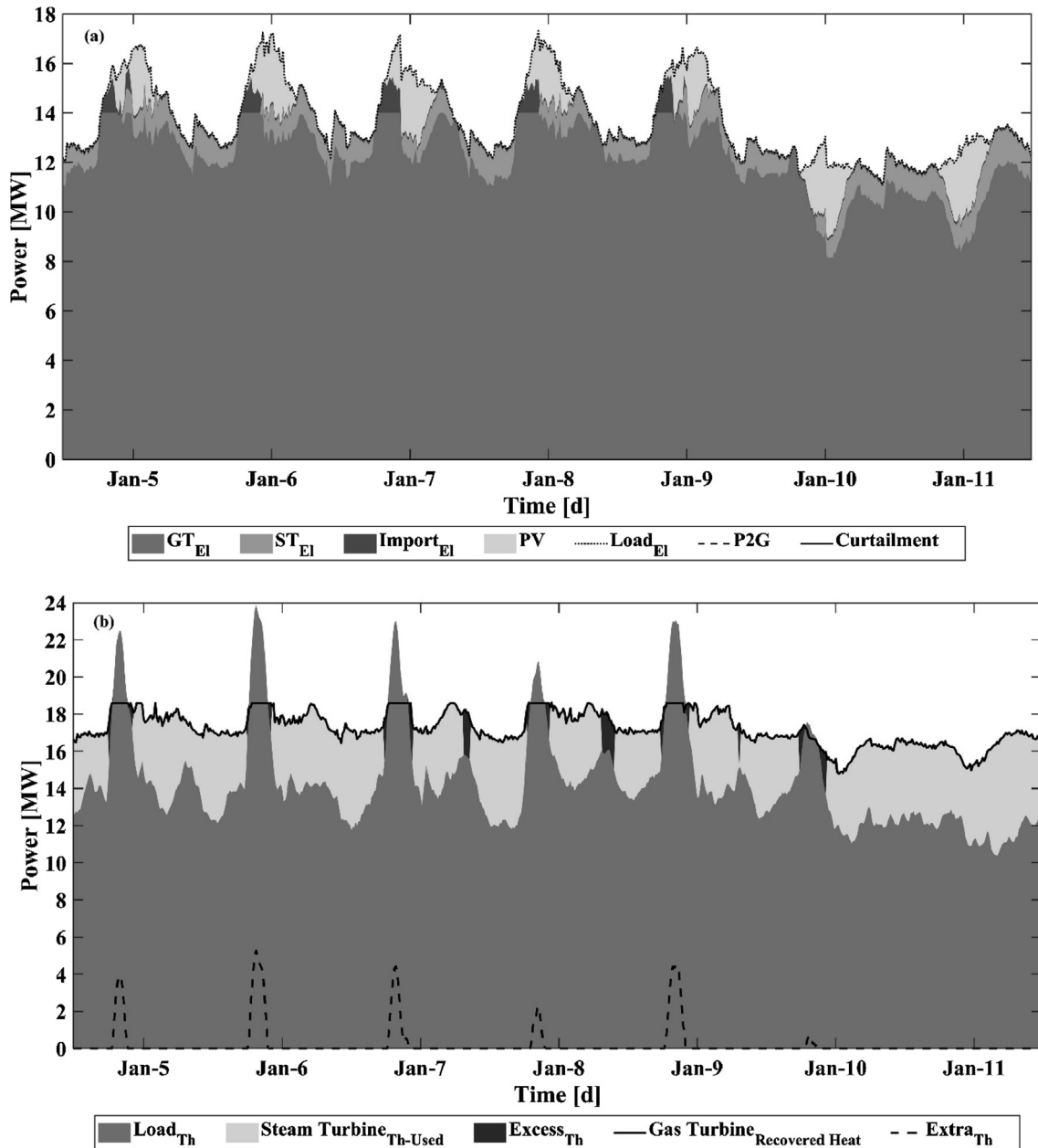


Fig. 10. Microgrid-SOE dispatch simulation results in a week of January (a) electric power balance (b) thermal power balance with the current 4 MW of PV installed capacity.

are simultaneous.

The last scenario reported in Figs. 13 and 14 for the two chosen weeks, is the scenario corresponding to 25 MW of installed PV capacity. In this scenario the peak PV power output reaches 19 MW and during many days this value is higher than the entire campus electrical demand. This situation of excess PV generation will worsen for scenarios with higher PV capacity that are not shown here. In the represented week, every day the gas turbine has to be turned down to the minimum operating condition while still every day massive solar excess power occurs. Electricity import is still necessary during the nights and during strong transient conditions.

According to Fig. 13(a), in the represented September week, we have excess electricity that is mostly stored in the form of hydrogen via P2G electric power consumption and a portion of it is curtailed since we selected to dispatch the minimum aggregated power capacity of SOE systems required to store 80% of the annual excess electric energy. According to Fig. 13(a), from September 2 to September 5,

approximately all the excess electric power is stored via P2G. However, in September 6 and 7, the amount of excess electric power is relatively high which forces all the dispatched SOE units to operate at full load resulting in 8 MW of P2G power consumption. As a result, we have around 4 MW and 6 MW of peak curtailment in these two days respectively. Also it should be noted that in the middle of all the days, there is a huge amount of excess thermal power due to relatively low thermal demand as well as high PV power which causes the steam turbine to be turned off. Moreover, in the represented September week, there is no need for extra thermal power since again the thermal demand can be totally supplied by the gas turbine recovered heat. It can be noticed that, when the heat demand is low enough, the presence of excess electricity and heat is often simultaneous as shown in Fig. 13. This fact will be exploited in a future study to supply steam to the electrolysis system generating it by recovering heat from gas turbine exhaust.

According to Fig. 14(a), in the represented January week, we have

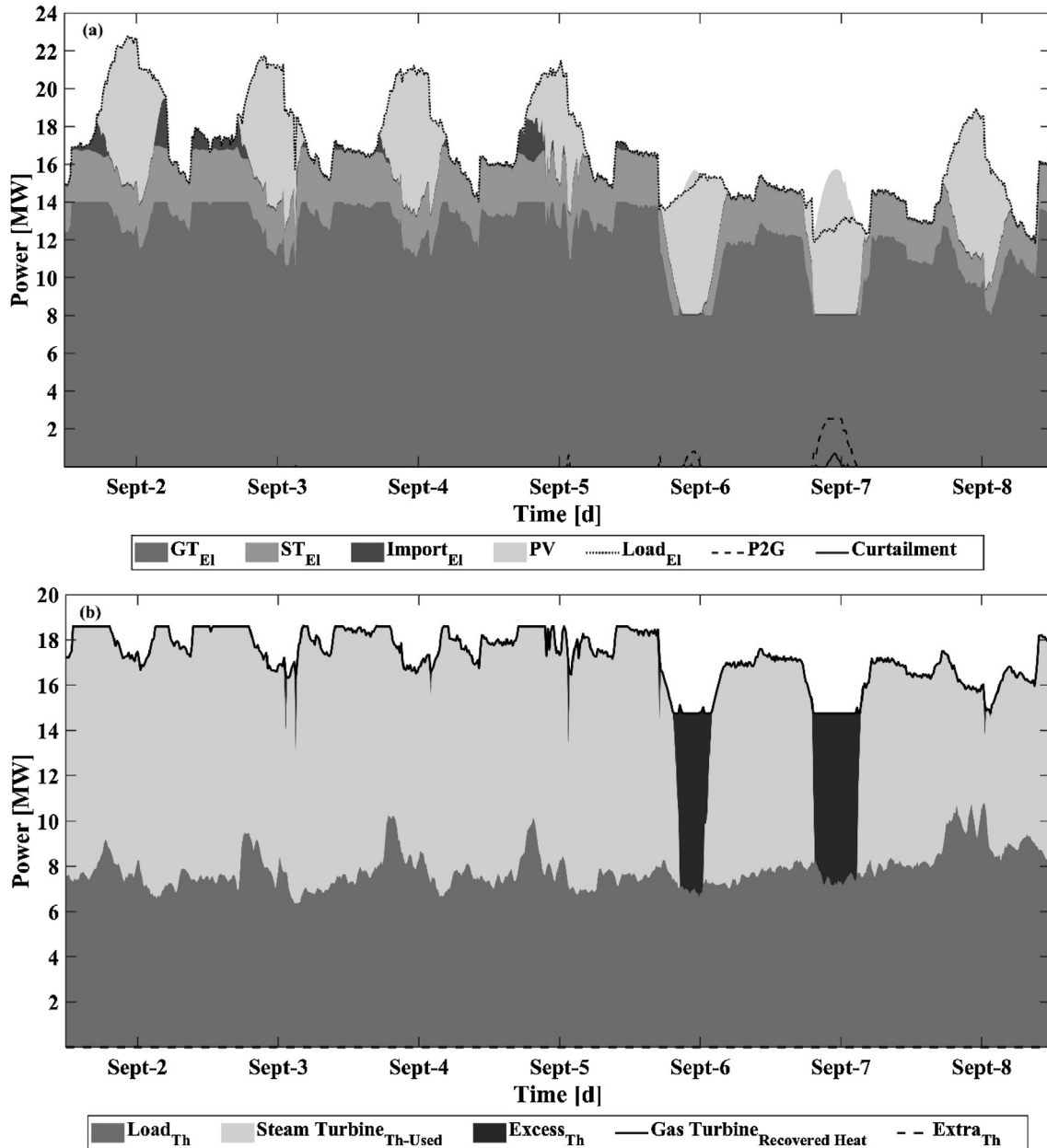


Fig. 11. Microgrid-SOE dispatch simulation results in a week of September (a) electric power balance, and (b) thermal power balance with 10 MW of PV installed capacity.

higher excess electricity compared to the September week especially from January 5 to January 8 (work days) due to lower electric demand. However, due to higher thermal demand in January, the excess thermal power is lower and there are some hours in which extra thermal energy is required to be supplied by additional natural gas combustion to meet the thermal demands of the campus.

In Fig. 15, the grid operation is represented in detail for the day of September 5. During this day cloud coverage appears from 10:00 to 11:30. As a consequence, PV output shows a drop from 13 to 1.3 MW followed by an increase to 16 MW in less than 2 h. In the same time-frame the gas turbine is not able to modulate its power output fast enough requiring electricity import to meet electrical demand from 10:30 to 11:30 during its ramp up and causing excess of electricity production during its ramp down between 11:30 and 12:15. As shown in Fig. 15(a), although the gas turbine output power reaches its minimum from 12:00 to 15:00, in this timeframe there is still excess power mainly consumed via P2G, since the PV power is higher than the

difference between the electric demand and the gas turbine minimum output power.

The same trends can be highlighted on a different scale looking at California net electricity demand, i.e., total electricity demand after wind and solar production, shown in Fig. 16 for a day in January 2019 [53]. At the current RES capacity present in the state of California, it is clear the phenomenon known as “the duck curve”: drop of power production requested from traditional fossil fuel plants and steep ramp up required in the late afternoon when the solar production decreases and the electricity demand reaches its peak. The suggested P2G system could be integrated to the statewide electricity system in a manner similar to that of the UCI microgrid, enabling conversion of a portion of renewable electricity to renewable hydrogen in the middle of the day. This implementation would not only reduce the required steep ramp up rates, but also utilize the produced renewable hydrogen in the existing gas plants to lower their carbon emissions. As a result, P2G conversion using high temperature SOE systems could more generally than the

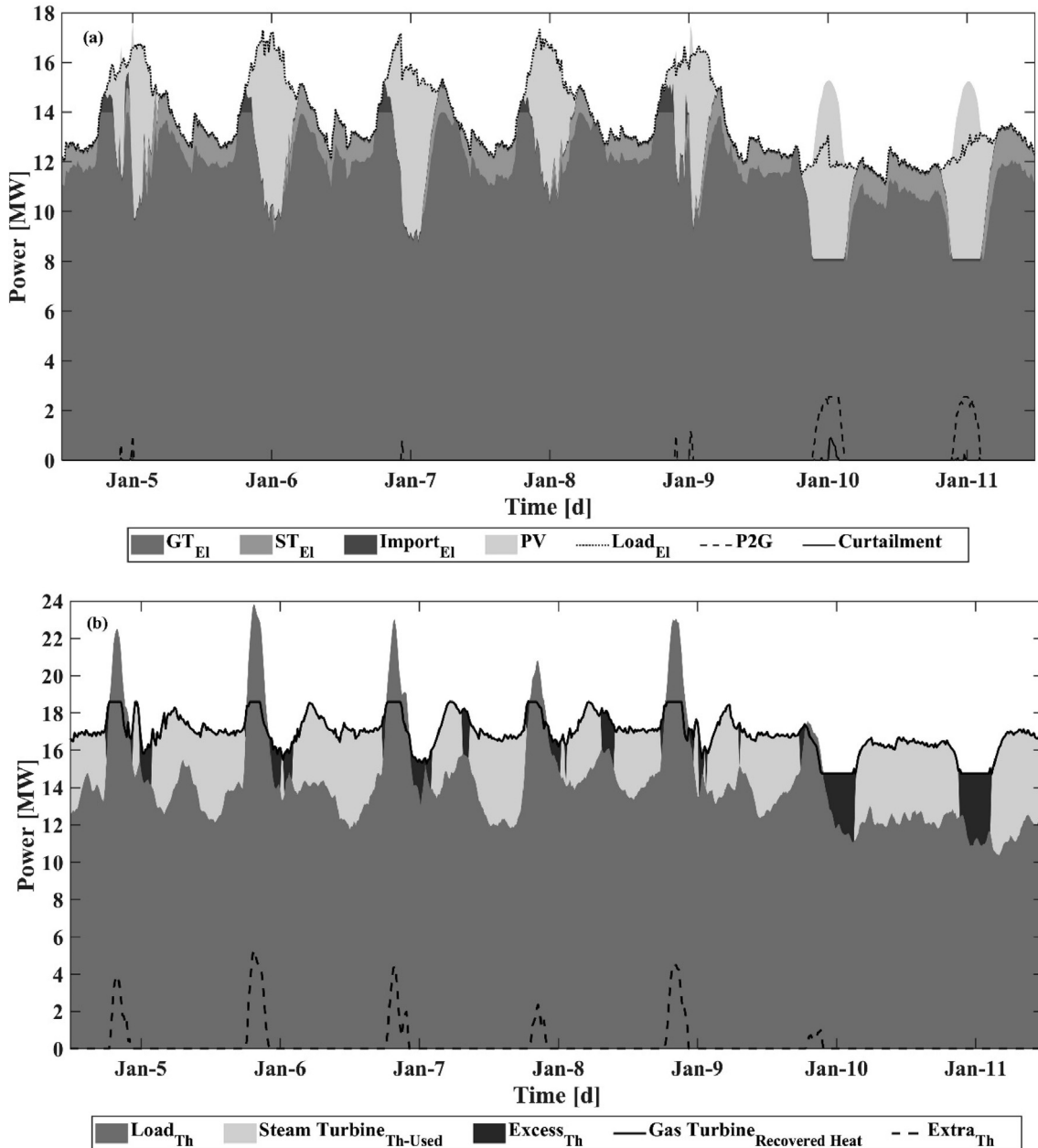


Fig. 12. Microgrid-SOE dispatch simulation results in a week of January (a) electric power balance, and (b) thermal power balance with 10 MW of PV installed capacity.

specific microgrid considered herein enable penetration of high RES in many grid networks to reduce the greenhouse gas emissions.

8.3. Hydrogen production

The estimations of the potential hydrogen production that could be obtained integrating high temperature SOE unit systems with the existing microgrid structure are presented in this section. Only scenarios relative to installed PV capacity higher than 10 MW are reported here because with lower capacity the electricity excess doesn't occur on a daily basis and the additional SOE capacity would mostly be wasted in idle mode. From the comparison of the annual hydrogen production shown in Fig. 17, it can be noticed that, as previously explained, scenarios with PV capacity higher than 15 MW would result in massive excess electricity levels and this increase is reflected by the hydrogen production potential that for a doubled PV capacity, from 10 to 20 MW, shows an almost nine times increase, passing from around 22 metric

tons per year to values higher than 191 tons per year.

These results can be analyzed in terms of the average annual efficiency of the electrolysis process evaluated according to Eq. (8).

$$\eta_{SOEC,Average} = \frac{m_{H_2,Annual} \times LHV_{H_2}}{E_{SOEC,Annual}} \quad (8)$$

where $m_{H_2,Annual}$ is the amount of hydrogen produced in one year, LHV_{H_2} is lower heating value of hydrogen and $E_{SOEC,Annual}$ is the total electrical energy delivered to the SOE units over the year. The average annual efficiency of the electrolysis process is approximately 70% for all the PV installed capacities considered ranging between 10 MW and 35 MW. This nearly constant efficiency is related to the electrolysis system design strategy proposed, which is made up of individual 300 kW SOE units that mostly operate at design conditions or are idle (not much part-load operation).

The simulation results show that sequential dispatch of 300 kW SOE systems into the UCI microgrid improves P2G efficiency compared to

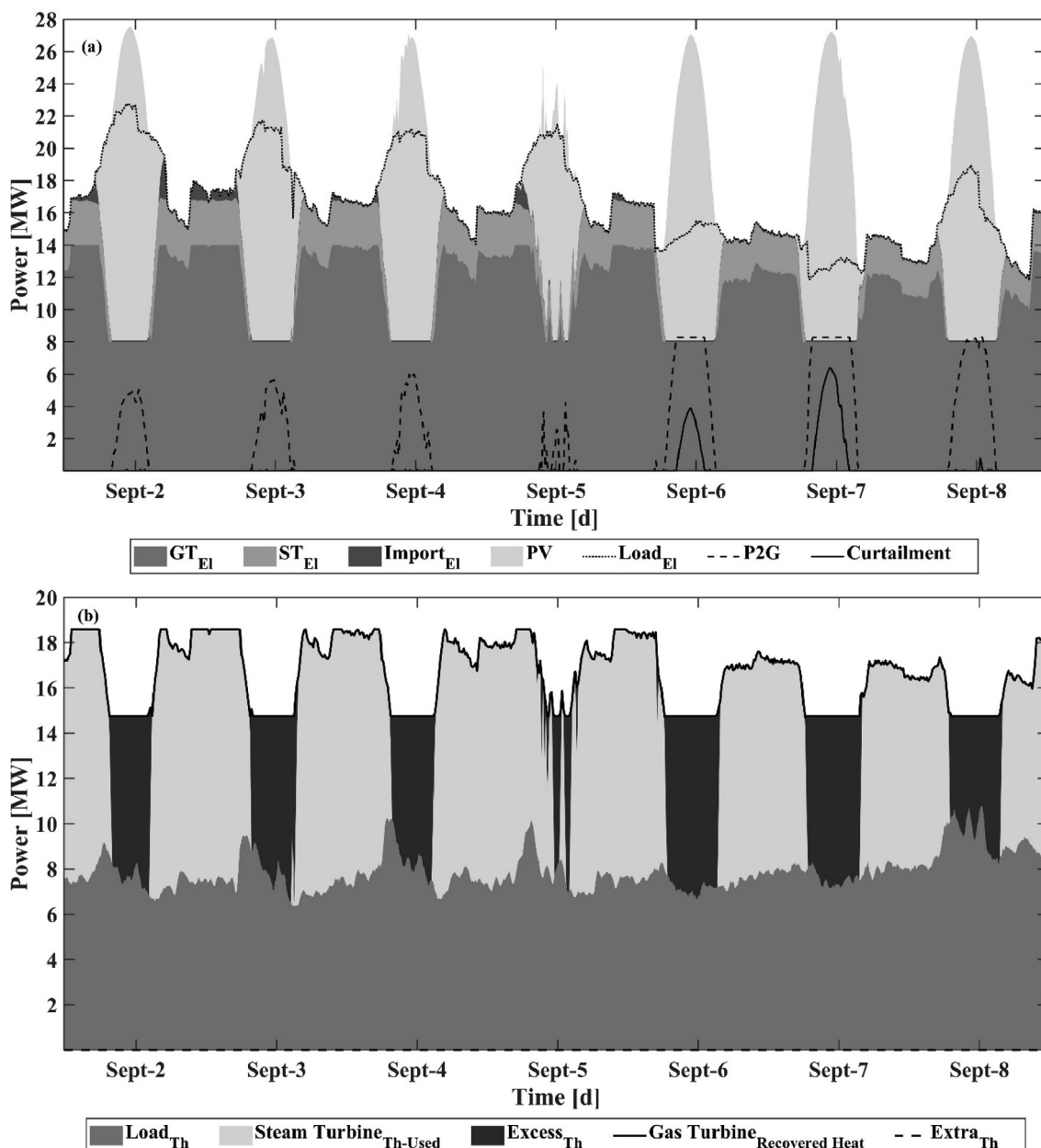


Fig. 13. Microgrid-SOE dispatch simulation results in a week of September (a) electric power balance, and (b) thermal power balance with 25 MW of PV installed capacity.

the currently available PEM electrolyzer producing hydrogen for the UCI campus. The simulated annual average efficiency of SOE systems for different PV penetration scenarios is 70% (LHV basis), which is significantly higher than the measured 50% (HHV basis) efficiency of the PEM electrolyzer that has been dynamically operated to integrate high PV use in the UCI microgrid [54].

8.4. On-site hydrogen utilization

The P2G system is based on the assumption that, injecting hydrogen into the natural gas distribution network, the hydrogen storage does not have to be built on site taking advantage of the very large existing storage volume represented by the natural gas distribution network. The amounts of hydrogen produced has been compared with possible on-site utilization capabilities such as the local hydrogen fueling station for fuel cell electric vehicles and the direct injection of the produced hydrogen in the gas turbine inlet to reduce the natural gas

consumption. The local fueling station maximum daily rated capacity is 180 kg of hydrogen and according to past years data, in 2017 were delivered 48,599 kg of hydrogen, resulting in an average daily delivery of 133 kg of hydrogen. This value more than doubled the amount of the previous year. Therefore, in the unlikely case that the local hydrogen demand for mobility does not increase in the near future, the hydrogen fueling station could consume the entire renewable hydrogen production from the microgrid excess electricity up to the scenario with 13 MW of PV capacity, in which the average daily hydrogen production is around 161 kg of hydrogen. In the case of 13 MW of PV capacity, 1.8 MW of SOE dispatched systems is required to store at least 80% of the annual excess electricity, and the annual production of the hydrogen would be around 59 metric tons.

Regarding the use of hydrogen as a fuel in the existing gas turbine, several studies have investigated the possibility of using a blend of natural gas and hydrogen to partially decarbonize the produced electricity and as a transitional solution toward future zero emissions

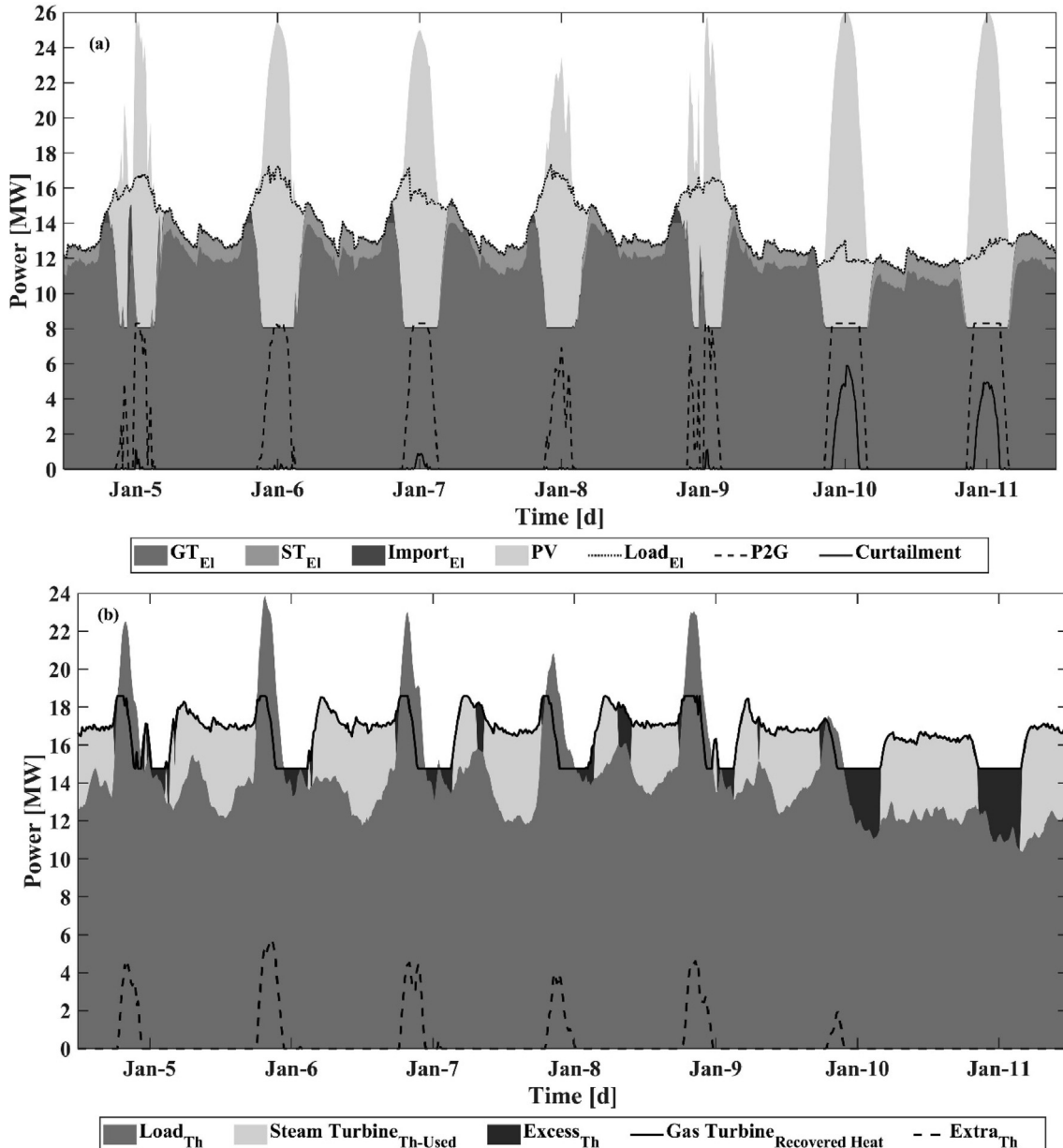


Fig. 14. Microgrid-SOE dispatch simulation results in a week of January (a) electric power balance (b) thermal power balance with 25 MW of PV installed capacity.

energy systems. A reference value for the hydrogen concentration limit that does not imply structural modification or important performance changes to existing devices is around 15% volumetric [48,49]. The molar heating value of the gas mixture with the reference hydrogen volume concentration can be estimated according to Eq. (9).

$$LHV_{mix} = x \times LHV_{H_2} + (1 - x) \times LHV_{NG} \quad (9)$$

where LHV_{H_2} and LHV_{NG} are the molar lower heating values of hydrogen and natural gas and x is the maximum volumetric hydrogen concentration. The maximum amount of hydrogen that could be injected into the gas turbine can be estimated with Eq. (10), assuming that feeding the gas turbine with the mixture of hydrogen and natural gas does not affect the efficiency.

$$n_{H2,GT} = x \times \frac{E_{GT,EI} / \eta_{GT,Average}}{LHV_{mix}} \quad (10)$$

where $E_{GT,EI}$ is the annual electric energy produced by the gas turbine, $\eta_{GT,Average}$ the average electrical efficiency of the gas turbine and x the

limit hydrogen volumetric concentration.

Fig. 18 shows the yearly amount of hydrogen production, yearly amount of hydrogen consumption by the gas turbine in the case of feeding the gas turbine with a gas mixture containing 15% volumetric hydrogen and 85% natural gas, and the yearly amount of hydrogen utilized in the local fueling station. As can be seen from Fig. 18, feeding the gas turbine with a gas mixture containing 15% volumetric hydrogen would suffice to consume the hydrogen produced up to the scenario with 32 MW of PV installed capacity. Moreover, the produced hydrogen associated with all of the PV capacity scenarios would be consumed in the case of using the produced hydrogen for feeding both the gas turbine and the fueling station. It is worth noting that as shown in Fig. 18, the blending limit of hydrogen decreases with increasing PV capacity deployment because the electrical energy produced by the gas turbine decreases, requiring overall lower fuel consumption. Fig. 19(a) shows the amount of reduced natural gas consumption in the gas turbine per year due to the 15% hydrogen blending with natural gas fed into the gas turbine. It shows that the integration of SOE systems to store 80% of

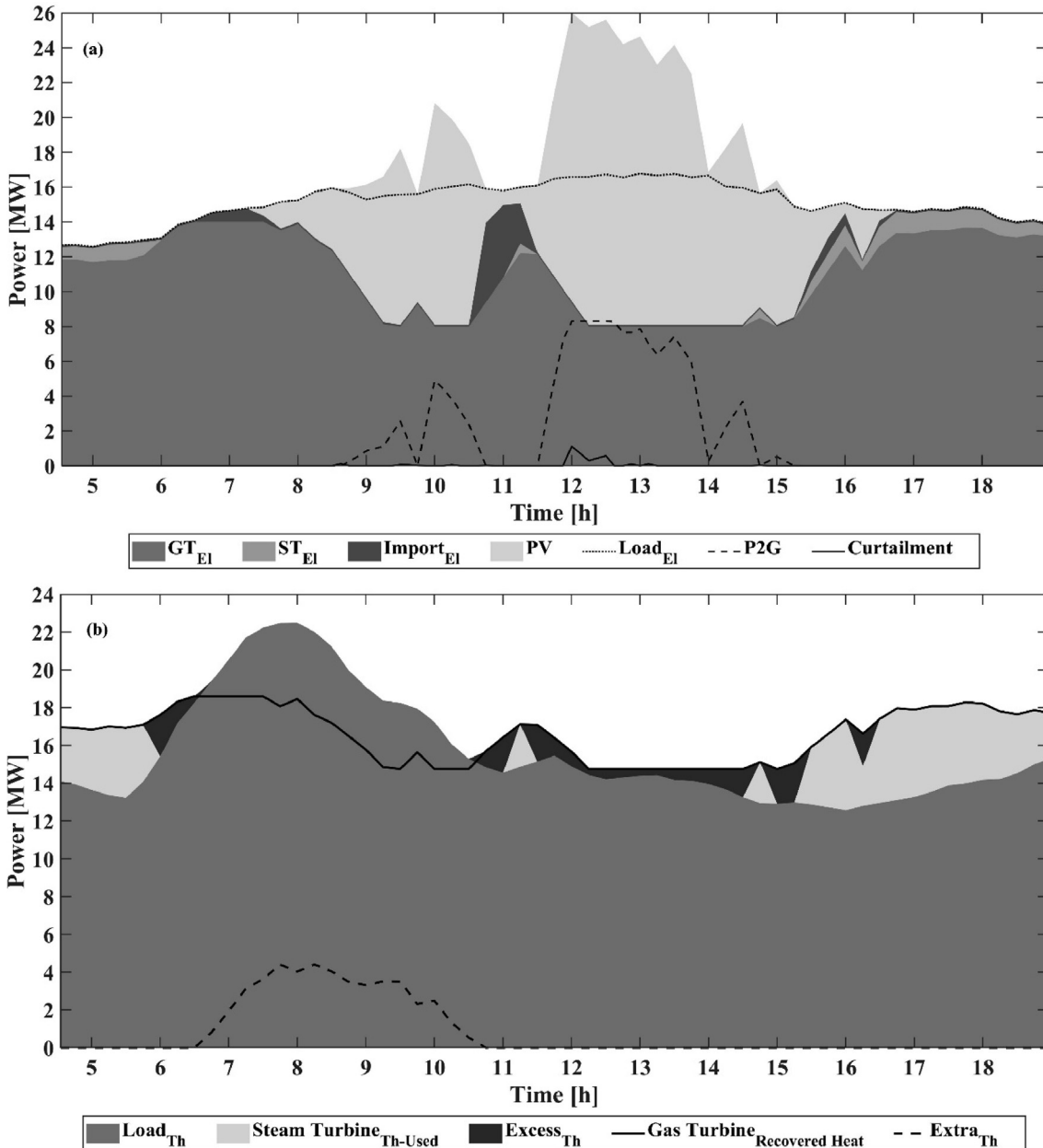


Fig. 15. Detail of microgrid operation during the day January 5 (a) electric power balance, and (b) thermal power balance with 25 MW of PV installed capacity.

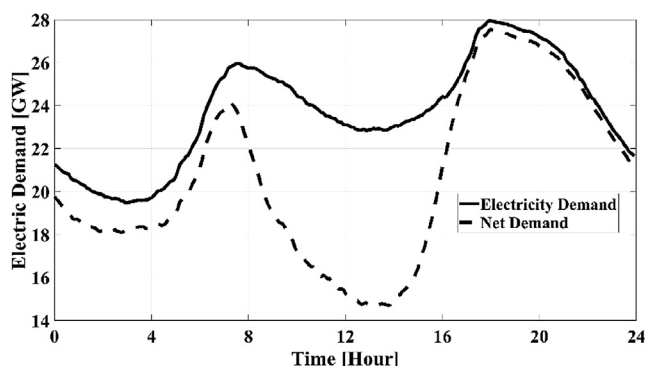


Fig. 16. Statewide California electricity demand and net demand for a day in January 2019 [53]

surplus electricity results in saving up to about 1200 metric tons of natural gas per year for the highest PV scenario. Thanks to the injection of hydrogen in the gas turbine, the annual natural gas consumption decreases between 120 metric tons to 1200 metric tons while the PV installed capacity increases between 10 MW and 35 MW respectively. As a consequence, blending hydrogen with the natural gas feeding the gas turbine results in annual 350 to 3500 metric tons reduction in carbon dioxide emissions for 10 MW to 35 MW PV scenarios respectively as shown in Fig. 19(b). On the other hand, integration of PV renewable generated electricity into the UCI microgrid also decreases the required electricity generation via gas turbine to meet the electric demand. This reduction also results in reducing natural gas consumption and carbon dioxide emissions. Microgrid simulation results show that there could be an annual 1560 to 3050 metric tons reduction in the natural gas consumption due to the increase in the PV share from the already existing 4 MW PV to 10 MW and 35 MW, respectively. Also, increasing the PV capacity from 4 MW to 10 MW and 35 MW would decrease the annual carbon dioxide emissions by 4300 to 8400 metric

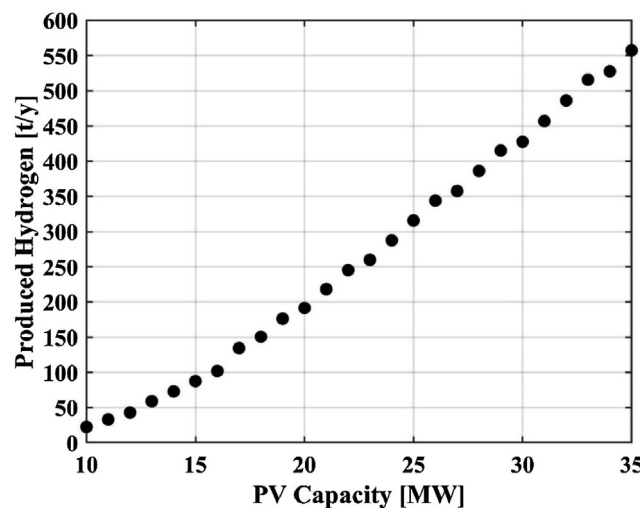


Fig. 17. Annual hydrogen production for different PV installed capacity.

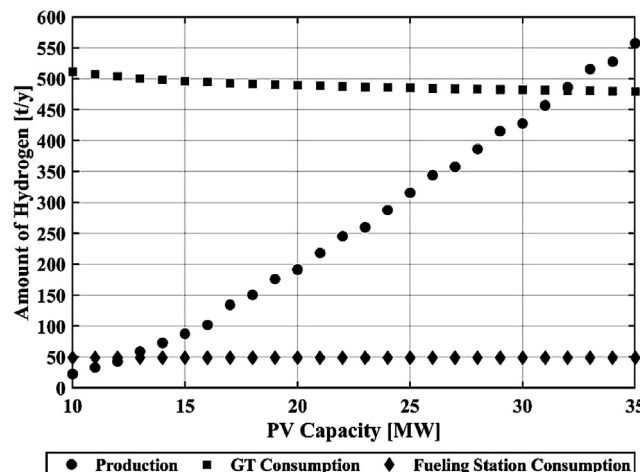


Fig. 18. Hydrogen production and possible on-site consumption for different PV installed capacity.

tons, respectively.

9. Summary and conclusions

The challenges of RES penetration have been investigated in the context of the University of California, Irvine campus microgrid, simulating the existing power plant operation and examining the effects of increasing renewable installed capacity. The limits of the microgrid power plant have been identified and would result in massive excess renewable electricity production, with no sensible increase in RES penetration in the campus electrical energy supply for renewable installed capacities higher than 15 MW, if no energy storage solution is implemented. The integration of a modular P2G system based on sequential dispatching of SOE systems into the campus microgrid has been modelled to evaluate the annual hydrogen production potential and the capability of the system to successfully absorb excess electricity from the additional renewable installations. The minimum aggregated power capacity of 300 kW dispatched SOE systems required to store at least 80% of the annual excess electricity is considered in each scenario. Utilization of the produced renewable hydrogen blended with natural gas as a fuel in UCI microgrid gas turbine, as well as the use of hydrogen in the local fueling station has been assessed. The results show that feeding the gas turbine with a gas mixture containing 15% volumetric hydrogen would suffice to consume all of the hydrogen produced up to the scenario with 32 MW of PV installed capacity. Moreover, the entire renewable hydrogen production in all of the PV capacity scenarios could be consumed on site considering both the feeding of the gas turbine with a gas mixture containing 15% by volume hydrogen and the delivery of hydrogen to fuel cell vehicles in the local fueling station. This would allow an increased share of renewable energy supply to the campus and accelerate decarbonization of the transportation sector of surrounding areas. In conclusion the deployment in the microgrid infrastructure of the additional PV capacity and the integration of the P2G system could reduce both natural gas consumption and carbon dioxide emissions. Up to 4250 metric tons (16%) of natural gas consumption and 11,900 tons (16%) of CO₂ emissions could be avoided.

CRediT authorship contribution statement

Paolo Colombo: Conceptualization, Methodology, Software, Formal analysis, Writing - original draft, Writing - review & editing, Visualization. **Alireza Saeedmanesh:** Conceptualization, Methodology, Software, Formal analysis, Writing - original draft, Writing - review & editing, Visualization. **Massimo Santarelli:** Writing - review & editing, Supervision, Project administration. **Jack Brouwer:** Conceptualization,

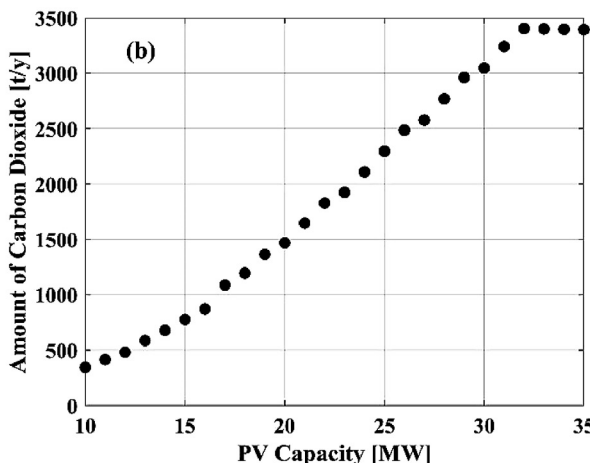
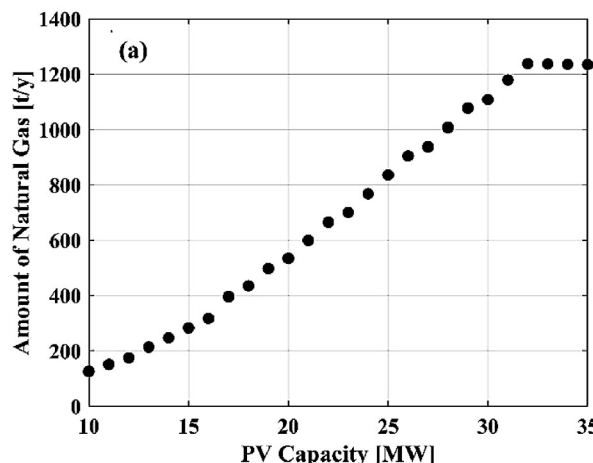


Fig. 19. (a) Yearly amount of avoided natural gas consumed by the gas turbine, and (b) yearly amount of reduction in CO₂ emission from the gas turbine for different PV installed capacity.

Writing - review & editing, Supervision, Project administration.

Declaration of Competing Interest

The authors declare that they have no known competing financial interests or personal relationships that could have appeared to influence the work reported in this paper.

Acknowledgements

The authors gratefully acknowledge the National Science Foundation (NSF) under the Integrated Food Energy Water Systems (INFEWS) program (Award No. 1639318) for partial funding support of this work.

Appendix A. Supplementary data

Supplementary data to this article can be found online at <https://doi.org/10.1016/j.enconman.2019.112322>.

References

- [1] Burke MJ, Stephens JC. Political power and renewable energy futures: A critical review. *Energy Res Soc Sci* 2018;35:78–93. <https://doi.org/10.1016/j.jerss.2017.10.018>.
- [2] Zong H, Cao Y, Liu Z. Energy security in Group of Seven (G7): a quantitative approach for renewable energy policy. *Energy Sources, Part B Econ Plan Policy* 2018;13:173–5. <https://doi.org/10.1080/15567249.2017.1422053>.
- [3] Perea-Moreno M-A, Hernandez-Escobedo Q, Perea-Moreno A-J. Renewable energy in urban areas: worldwide research trends. *Energies* 2018;11:577. <https://doi.org/10.3390/en11030577>.
- [4] Streicher W. Energy Efficiency and Renewable Energy: the key factors for a sustainable future. *Renew Energy Sustain Dev* 2018;4:1. <https://doi.org/10.21622/resd.2018.04.1.001>.
- [5] Konstantin P, Konstantin M. *Power Generation from Renewable Energies*. Power Supply Ind., Cham: Springer International Publishing; 2018. p. 89–136. doi: [10.1007/978-3-319-72305-1_5](https://doi.org/10.1007/978-3-319-72305-1_5).
- [6] Eichman JD, Mueller F, Tarroja B, Schell LS, Samuelsen S. Exploration of the integration of renewable resources into California's electric system using the Holistic Grid Resource Integration and Deployment (HiGRID) tool. *Energy* 2013;50:353–63. <https://doi.org/10.1016/j.energy.2012.11.024>.
- [7] Assareh E, Nedaei M. A metaheuristic approach to forecast the global carbon dioxide emissions. *Int J Environ Stud* 2018;75:99–120. <https://doi.org/10.1080/00207233.2017.1374075>.
- [8] Hernández-Escobedo Q, Perea-Moreno A-J, Manzano-Agudelo F. Wind energy research in Mexico. *Renew Energy* 2018;123:719–29. <https://doi.org/10.1016/j.renene.2018.02.101>.
- [9] Rodríguez-Urrego D, Rodríguez-Urrego L. Photovoltaic energy in Colombia: current status, inventory, policies and future prospects. *Renew Sustain Energy Rev* 2018;92:160–70. <https://doi.org/10.1016/j.rser.2018.04.065>.
- [10] Gotzens F, Heinrichs H, Hake JF, Allelein HJ. The influence of continued reductions in renewable energy cost on the European electricity system. *Energy Strateg Rev* 2018;21:71–81. <https://doi.org/10.1016/j.esr.2018.04.007>.
- [11] International Renewable Energy Agency (IRENA). Renewable Power Generation Costs in 2017; 2018.
- [12] Nottou G, Nivet ML, Voyant C, Paoli C, Darras C, Motte F, et al. Intermittent and stochastic character of renewable energy sources: Consequences, cost of intermittence and benefit of forecasting. *Renew Sustain Energy Rev* 2018;87:96–105. <https://doi.org/10.1016/j.rser.2018.02.007>.
- [13] Mazza A, Bompard E, Chicco G. Applications of power to gas technologies in emerging electrical systems. *Renew Sustain Energy Rev* 2018;92:794–806. <https://doi.org/10.1016/j.rser.2018.04.072>.
- [14] Lewandowska-Bernat A, Desideri U. Opportunities of power-to-gas technology in different energy systems architectures. *Appl Energy* 2018;228:57–67. <https://doi.org/10.1016/j.apenergy.2018.06.001>.
- [15] Blanco H, Faaij A. A review at the role of storage in energy systems with a focus on Power to Gas and long-term storage. *Renew Sustain Energy Rev* 2018;81:1049–86. <https://doi.org/10.1016/j.rser.2017.07.062>.
- [16] Walker SB, Mukherjee U, Fowler M, Elkamel A. Benchmarking and selection of Power-to-Gas utilizing electrolytic hydrogen as an energy storage alternative. *Int J Hydrogen Energy* 2016;41:7717–31. <https://doi.org/10.1016/j.ijhydene.2015.09.008>.
- [17] Saeedmanesh A, Mac Kinnon MA, Brouwer J. Hydrogen is essential for sustainability. *Curr Opin Electrochem* 2018;12:166–81. <https://doi.org/10.1016/j.colelec.2018.11.009>.
- [18] Davis SJ, Lewis NS, Shaner M, Aggarwal S, Arent D, Azevedo IL, et al. Net-zero emissions energy systems. *Science* 2018(80-). <https://doi.org/10.1126/science.aas9793>. 360:eaas9793.
- [19] Yazdani S, Deymi-Dashtebayaz M, Salimipour E. Comprehensive comparison on the ecological performance and environmental sustainability of three energy storage systems employed for a wind farm by using an energy analysis. *Energy Convers Manag* 2019;1–11. <https://doi.org/10.1016/j.enconman.2019.04.021>.
- [20] He C, Liu T, Wu L, Shahidehpour M. Robust coordination of interdependent electricity and natural gas systems in day-ahead scheduling for facilitating volatile renewable generations via power-to-gas technology. *J Mod Power Syst Clean Energy* 2017;5:375–88. <https://doi.org/10.1007/s40565-017-0278-z>.
- [21] Yang Z, Gao C, Zhao M. Coordination of integrated natural gas and electrical systems in day-ahead scheduling considering a novel flexible energy-use mechanism. *Energy Convers Manag* 2019;196:117–26. <https://doi.org/10.1016/j.enconman.2019.05.109>.
- [22] Brandon NP, Kurban Z. Clean energy and the hydrogen economy. *Phil Trans R Soc A* 2017;375:20160400. <https://doi.org/10.1098/rsta.2016.0400>.
- [23] Safari F, Dincer I. Assessment and optimization of an integrated wind power system for hydrogen and methane production. *Energy Convers Manag* 2018;177:693–703. <https://doi.org/10.1016/j.enconman.2018.09.071>.
- [24] Wang L, Pérez-Fortes M, Madi H, Diethelm S, herle J, Van Maréchal F. Optimal design of solid-oxide electrolyzer based power-to-methane systems: a comprehensive comparison between steam electrolysis and co-electrolysis. *Appl Energy* 2018;211:1060–79. <https://doi.org/10.1016/j.apenergy.2017.11.050>.
- [25] Luo Y, Wu X, Yu, Shi Y, Ghoniem AF, Cai N. Exergy analysis of an integrated solid oxide electrolysis cell-methanation reactor for renewable energy storage. *Appl Energy* 2018;215:371–83. <https://doi.org/10.1016/j.apenergy.2018.02.022>.
- [26] Jun C, Yu H. Water electrolysis based on renewable energy for hydrogen production. *Chinese J Catal* 2018;39:390–4. <https://doi.org/10.1016/j.s1872>.
- [27] AlZahrani AA, Dincer I. Modeling and performance optimization of a solid oxide electrolysis system for hydrogen production. *Appl Energy* 2018;225:471–85. <https://doi.org/10.1016/j.apenergy.2018.04.124>.
- [28] AlZahrani AA, Dincer I. Thermodynamic and electrochemical analyses of a solid oxide electrolyzer for hydrogen production. *Int J Hydrogen Energy* 2017;42:21404–13. <https://doi.org/10.1016/j.ijhydene.2017.03.186>.
- [29] California Hydrogen Business Council 3438 Merrimac Road, Los Angeles C 90049. Power-to-Gas: The Case for Hydrogen; 2015.
- [30] Pellow MA, Emmott CJM, Barnhart CJ, Benson SM. Hydrogen or batteries for grid storage? A net energy analysis. *Energy Environ Sci* 2015;8:1938–52. <https://doi.org/10.1039/C4EE04041D>.
- [31] Maton J-P, Zhao L, Brouwer J. Dynamic modeling of compressed gas energy storage to complement renewable wind power intermittency. *Int J Hydrogen Energy* 2013;38:7867–80. <https://doi.org/10.1016/j.ijhydene.2013.04.030>.
- [32] Uusitalo V, Väistönen S, Inkeri E, Soukka R. Potential for greenhouse gas emission reductions using surplus electricity in hydrogen, methane and methanol production via electrolysis. *Energy Convers Manag* 2017;134:125–34. <https://doi.org/10.1016/j.enconman.2016.12.031>.
- [33] Ghabai K, Ben-Fares FZ. Power-to-methane: a state-of-the-art review. *Renew Sustain Energy Rev* 2018;81:433–46. <https://doi.org/10.1016/j.rser.2017.08.004>.
- [34] Shaffer B, Tarroja B, Samuelsen S. Dispatch of fuel cells as Transmission Integrated Grid Energy Resources to support renewables and reduce emissions. *Appl Energy* 2015;148:178–86. <https://doi.org/10.1016/j.apenergy.2015.03.018>.
- [35] ENEL green power 2017:1–482. https://www.enel.com/content/dam/enel-com/governance_pdf/reports/annual-financial-report/2017/annual-report-2017.pdf.
- [36] Stone Edge Farm MicroGrid n.d. <https://sefmicrogrid.com/>.
- [37] First Power-to-Gas projects in US feature Proton electrolyzers. *Fuel Cells Bull* 2015; 2015: 9. doi: 10.1016/S1464-2859(15)30124-3.
- [38] Duíci N, da Graça Carvalho M. Increasing renewable energy sources in island energy supply: case study Porto Santo. *Renew Sustain Energy Rev* 2004;8:383–99. <https://doi.org/10.1016/j.rser.2003.11.004>.
- [39] Lin J-H, Wu Y-K, Lin H-J. Successful experience of renewable energy development in several offshore islands. *Energy Procedia* 2016;100:8–13. <https://doi.org/10.1016/j.egypro.2016.10.137>.
- [40] Petipas F, Brisse A, Bouallou C. Model-based behaviour of a high temperature electrolyser system operated at various loads. *J Power Sources* 2013;239:584–95. <https://doi.org/10.1016/j.jpowsour.2013.03.027>.
- [41] Saeedmanesh A, Colombo P, McLarty D, Brouwer J. Dynamic behavior of a solid oxide steam electrolyzer system using transient photovoltaic generated power for renewable hydrogen production. 041008 J Electrochim Energy Convers Storage 2019;16. <https://doi.org/10.1115/1.4043340>.
- [42] Sanz-Bermejo J, Muñoz-Antón J, Gonzalez-Aguilar J, Romero M. Part load operation of a solid oxide electrolysis system for integration with renewable energy sources. *Int J Hydrogen Energy* 2015;40:8291–303. <https://doi.org/10.1016/j.ijhydene.2015.04.059>.
- [43] Buttler A, Spleithoff H. Current status of water electrolysis for energy storage, grid balancing and sector coupling via power-to-gas and power-to-liquids: a review. *Renew Sustain Energy Rev* 2018;82:2440–54. <https://doi.org/10.1016/j.rser.2017.09.003>.
- [44] Ebbesen SD, Jensen SH, Hauch A, Mogensen MB. High temperature electrolysis in alkaline cells, solid proton conducting cells, and solid oxide cells. *Chem Rev* 2014;114:10697–734. <https://doi.org/10.1021/cr5000865>.
- [45] Samuelsen S, Mueller F, Eichman J, Tarroja B. Piloting the integration and use of renewables to achieve a flexible and secure energy infrastructure. *Calif Energy Comm* 2013.
- [46] McLarty D, Civit Sabate C, Brouwer J, Jabbari F. Micro-grid energy dispatch optimization and predictive control algorithms: A UC Irvine case study. *Int J Electr Power Energy Syst* 2015;65:179–90. <https://doi.org/10.1016/j.ijepes.2014.09.039>.
- [47] Chandan V, Do A, Jin B, Jabbari F, Brouwer J, Akrotirianakis I, et al. Modeling and optimization of a combined cooling, heating and power plant system. *Am. Control Conf.* 2012;3069–74. <https://doi.org/10.1109/ACC.2012.6315606>.

- [48] Shaffer B, Tarroja B, Samuelsen S. Advancing Toward Sustainability Goals at the University of California, Irvine. Proc. ASME 2014 8th Int. Conf. Energy Sustain., Boston, Massachusetts; 2014, p. 1–14. doi: 10.1115/ES2014-6453.
- [49] Do A-TV. Performance and Controls of Gas Turbine-Driven Combined Cooling Heating and Power Systems for Economic Dispatch. University of California, Irvine, 2013.
- [50] Prous Y.I.I. R. Dynamic dispatch and control of hydrogen energy storage from solar power in microgrids. Irvine: University of California; 2015.
- [51] Hoeschele M, Weitzel E. Hot water distribution system model enhancements alliance for residential building. Innovation (ARBI) 2012.
- [52] Petipas F, Brisse A, Bouallou C. Modelled behaviour of a high temperature electrolyser system coupled with a solar farm. Chem Eng Trans 2015;45. <https://doi.org/10.3303/CET1545170>.
- [53] California ISO - Todays Outlook n.d. <http://www.caiso.com/TodaysOutlook/Pages/default.aspx>.
- [54] Stansberry J, Hormaza Mejia A, Zhao L, Brouwer J. Experimental analysis of photovoltaic integration with a proton exchange membrane electrolysis system for power-to-gas. Int J Hydrogen Energy 2017;42:30569–83. <https://doi.org/10.1016/j.ijhydene.2017.10.170>.